Chemical Engineering Journal 499 (2024) 155946

Contents lists available at ScienceDirect

Chemical Engineering Journal

journal homepage: www.elsevier.com/locate/cej

Plasma-assisted NH_3 cracking in warm plasma reactors for green H_2 production

Igor Fedirchyk *, Ivan Tsonev, Rubén Quiroz Marnef, Annemie Bogaerts

PLASMANT, Department of Chemistry, University of Antwerp, Universiteitsplein 1, BE-2610 Wilrijk, Antwerp, Belgium

ARTICLE INFO

Keywords:
Plasma-assisted NH_3 cracking
Plasma reactors
Warm plasma
H_2 production from NH_3

ABSTRACT

NH_3 is emerging as a carrier of green H_2, but it requires a green and economical NH_3 cracking process based on renewable energy. Plasma technology is promising for this purpose, as it can crack NH_3 without the need for a catalyst and is highly compatible with renewable electricity, reducing the environmental footprint of the cracking process. This work investigates the NH_3 cracking performance of four different warm plasma reactors with different configurations and operating in a wide range of conditions. We show that the NH_3 conversion in warm plasma reactors is primarily determined by the specific energy input, with the main difference observed in the energy cost (EC) of cracking. The lowest EC obtained is 146 kJ/mol but at a conversion of only 8 %. A more reasonable conversion of around 50 % yields an EC of around 200 kJ/mol in two of the reactors investigated. Plasma reactors operating at higher feed flow rates are more efficient and yield a higher H_2 production rate. Our data indicate that NH_3 cracking in these warm plasma reactors occurs mainly via thermal chemistry, with non-thermal plasma chemistry playing a less prominent role. NH_3 decomposes not only inside the plasma core but also in a hot volume around it, which reduces the EC. Our study shows that warm plasmas are significantly more efficient for NH_3 cracking than cold plasmas, even when the latter are combined with catalysts.

1. Introduction

The increased demand for hydrogen (H_2) in the near future due to the transition to renewable and carbon-free energy is already established in the energy transition strategies of various countries. For example, H_2 plays a significant role in the EU's long-term strategy for a climate-neutral economy [1]. However, the limited access to renewable energy sources for green H_2 production means that some European countries will need to import large volumes of green H_2 to achieve the EU 2050 climate neutrality target [1]. This requires the ability to transport it over long distances and store it in large quantities for extended periods. Currently, H_2 is most often stored in gaseous form in pressure vessels at pressures of 20 – 30 MPa. However, due to its low molar weight, storing gaseous H_2 is severely limited by its poor mass storage efficiency, which can only be improved by storing it at higher pressure (70 MPa or higher) via cryogenic compression [2].

Due to the complex and costly nature of H_2 storage and transportation, there is a need for a suitable H_2 carrier that can mitigate these problems. From all potential H_2 carriers, NH_3 is the main carbon-free option that can be produced using only renewable energy. One advantage of NH_3 is its high volumetric and gravimetric hydrogen density. Another advantage is that NH_3 is a chemical with high demand for fertiliser production, and, as a result, it has a well-established transportation infrastructure.

The production of H_2 using electricity is currently expensive. This might raise questions about the feasibility of storing it in NH_3 and then converting NH_3 back into H_2 using electricity, based on the current infrastructure. However, while the economic assessment of NH_3 generation from renewable H_2 is beyond the scope of this article, it is a rapidly developing field with a lot of interest from governmental and commercial stakeholders. Furthermore, H_2 can be produced in areas with abundant and cheap renewable electricity, where it will be converted to NH_3, which can then be transported over long distance to areas with more expensive energy [3].

Although technological solutions exist for NH_3 production and transportation, the H_2 delivery scheme via NH_3 requires an energy-efficient technology for cracking NH_3 into H_2 and N_2 that is preferably fully compatible with renewable energy sources, which currently is not available [4]. Thermo-catalytic cracking is the most studied NH_3 decomposition option, but to be thermodynamically favoured, it

* Corresponding author.
E-mail address: igor.fedirchyk@uantwerpen.be (I. Fedirchyk).

https://doi.org/10.1016/j.cej.2024.155946
Received 19 June 2024; Received in revised form 23 August 2024; Accepted 16 September 2024
Available online 19 September 2024

requires high temperatures (>300 °C), with 400–600 °C needed to achieve NH_3 conversion above 99.5 % [5]. Heating the gas feed and catalyst bed to these temperatures consumes additional energy and decreases the round-trip efficiency. Reducing the process temperature is possible by selecting the most effective catalysts, which include expensive materials, such as ruthenium. In addition, highly effective Ru-based catalysts have been shown to suffer from deactivation during NH_3 cracking due to Ru sintering and diffusion into the support [5], negatively impacting the efficiency and costs of the process. The best commercial performance of catalytic NH_3 cracking was claimed by Haldor Topsøe A/S, stating 95 % NH_3 conversion at an energy cost (EC) of approximately 65 kJ/mol [6] using a process derived from the technology designed for the production of high-purity H_2 in metallurgy and heavy water production.

The EC is an important parameter that defines the energy efficiency and minimal operational costs of the NH_3 cracking process. The aim of the NH_3 cracking process lies in extracting H_2 back from its carrier at the lowest possible energy consumption, which can be effectively described by the EC. Additionally, the EC gives a common point of comparison between the estimated efficiency of the different NH_3 conversion processes that are independent of process specifics, such as the presence of a catalyst or the method for heating the feed gas. In our plasma process, it is defined by the (plasma) energy needed to convert a certain amount of NH_3 (see Eqs. (2) and (5) below).

Plasma technology offers a promising alternative for NH_3 decomposition. Plasma is a partially ionised gas comprising molecules, electrons, ions, radicals, and excited species. The electrons activate the gas molecules, creating reactive species that allow endothermic reactions, like NH_3 cracking, to occur at milder conditions. Plasmas are commonly split into two types: thermal, in which the temperatures of all plasma species are equal, and non-thermal, in which there is a high degree of non-equilibrium with lighter electrons having much higher temperature than heavier ions and neutral particles. From a plasma chemistry point of view, non-thermal plasmas can be further split into either cold plasmas, which have a strong non-equilibrium between translational, rotational, and vibrational temperatures of plasma species, with gas temperatures typically around room temperature up to 1000 K, or warm plasmas, in which these three temperatures are almost equal to each other, with gas temperatures usually between 1000 K and 6000 K, and the electron temperature being significantly higher. The classification of plasma as cold or warm is thus mainly determined by the gas temperature. The four plasma types investigated in this work belong to the category of “warm plasmas”.

Using plasma for NH_3 cracking can provide several advantages over thermo-chemical cracking. Warm plasmas can easily heat the gas to high temperatures that are not easily achievable in traditional reactors, allowing thermal NH_3 cracking to occur more rapidly. The absence of catalysts reduces the costs of the process and removes possible problems caused by catalyst deactivation. In addition, it allows for a more compact cracking setup, expanding the range of possible applications. Last but not least, plasma can be created by using electricity and can be quickly switched on/off, which combines perfectly with the intermittent nature of renewable electricity, allowing the process to produce green H_2.

Table 1
Overview of various plasma reactors used for NH_3 cracking, indicating the plasma type (thermal, warm or cold), operating conditions (with or without catalyst, preheating, power, feed flow rate, NH_3 concentration in the feed, specific energy input (SEI) per mole of NH_3 in feed gas; see Eq. (2) below), and the performance (in terms of NH_3 conversion and energy cost (EC)), collected from the literature. RF=inductively coupled RF plasma, DBD=dielectric barrier discharge, AC=alternating current, GA=gliding arc, NTAP=non-thermal arc plasma, MW=microwave plasma.

Plasma reactor	Plasma type	Catalyst and/or preheating	Power (W)	Feed flow rate (L/min)	NH_3 concentration (%)	SEI (per NH_3) (kJ/mol)	NH_3 conversion (%)	EC (per NH_3) (kJ/mol)	Ref.
RF	thermal	none	25,000	184.6	14.6	1245	91.3	1364	[7]
RF	thermal	none	25,000	171.6	8.2	2402	98.7	2433	[7]
DBD	cold	Co/fumed SiO_2, heated to 380 °C	10	0.04	100	336	98	343	[8]
DBD	cold	1.5 % Ru/La_2O_3, heated to 380 °C	12	0.04	100	404	99.9	404	[9]
DBD	cold	1.5 % Ru/La_2O_3	12	0.04	100	404	20	2017	[9]
DBD	cold	6Fe-4Ni, heated to 500 °C	48.2	0.12	100	540	100	540	[10]
DBD	cold	heated to 500 °C	48.2	0.12	100	540	22	2455	[10]
DBD	cold	Ni, heated to 700 °C	500	1.5	100	449	75	598	[11]
DBD	cold	2 % Ru/Al_2O_3 with SA-600 A zeolite and hydrogen membrane	500	1	100	672	96.6	696	[12]
DBD	cold	none	500	0.5	100	1345	2.7	49,809	[12]
DBD	cold	Co/fumed SiO_2	22	0.04	100	749	99.2	755	[13]
DBD	cold	none	19	0.04	100	629	6	10,490	[13]
DBD	cold	Fe/Fe_4N/Fe_3N, heated to 410 °C	25	0.04	100	841	100	841	[14]
DBD	cold	heated to 470 °C	25	0.04	100	841	9.7	8665	[14]
DBD	cold	Mo_2N	15.8	0.3	100	888	100	888	[15]
DBD	cold	Mo_2N, heated to 490 °C	40	0.04	100	1345	92	1462	[16]
DBD	cold	heated to 490 °C	40	0.04	100	1345	33	4075	[16]
DBD	cold	none	300	1	100	403	19	2123	[17]
DBD	cold	$MgAl_2O_4$	21	0.075	100	377	15.1	2494	[18]
DBD	cold	none	21	0.075	100	377	5	7531	[18]
DBD	cold	hydrogen membrane	400	0.5	100	1076	22	4890	[19]
DBD	cold	none	10	0.009	100	1494	20	7471	[20]
DBD	cold	none	11	0.03	67	736	29	2538	[21]
DBD	cold	Ni, heated to 435 °C	20	0.05	15	3586	99.6	3601	[22]
DBD	cold	none	50	0.2	4.9	6904	100	6904	[23]
DBD	cold	heated to 325 °C	5	1	1	672	8	8405	[24]
DBD	cold	none	15	0.05	2	19,973	82	24,357	[25]
DBD	cold	none	121	1	0.5	32,545	21.5	151,372	[26]
AC	warm	none	24.3	0.04	100	817	98	834	[27]
GA	warm	none	250	3.667	100	90	20.7	443	[28]
GA	warm	none	340	3	18	847	55	1540	[28]
NTAP	warm	none	700	30	100	31	16	196	[29]
NTAP	warm	15 % NiO/Al_2O_3	700	30	100	31	20	157	[29]
GA	warm	Ba-Co/CeO_2	300	3	50	269	70	384	[30]
MW	warm	none	150	2	2.3	4348	75.6	5752	[31]

NH_3 cracking using plasma technology is gaining increasing interest in recent years. Table 1 presents an overview of the conditions for NH_3 cracking and the performance of selected plasma reactors from the literature. Early experiments with thermal radio frequency (RF) plasma [7] showed low energy efficiency and limited practicality due to using NH_3 diluted in Ar/H_2 and significant heat losses. However, there has been a recent surge of interest in NH_3 cracking using various plasmas [8–31], particularly with dielectric barrier discharge (DBD) plasmas [8–26], sometimes combined with catalysts [8–10,12–16,18,22]. Nevertheless, these plasmas are generally much less energy efficient than warm plasmas, such as gliding arc (GA) plasmas [32], which can decompose NH_3 more easily due to the higher plasma temperatures, reaching and exceeding 3000 K in the core [33]. This can be inferred from the difference between the minimum EC of DBD reactors without catalyst (2123 kJ/mol [17]; see Table 1), which is more than ten times higher than the lowest EC in warm plasma reactors without catalyst (196 kJ/mol [29]; see Table 1).

Warm plasmas were not so often used for NH_3 cracking up to now. An AC discharge [27] demonstrated high NH_3 conversion (98 %) but at a high EC (834 kJ/mol). NH_3 cracking in MW plasma has also shown high EC (5752 kJ/mol) [31] due to a significant dilution of NH_3 with Ar. Two interesting papers [28,29] on warm plasmas, i.e., gliding arc (GA) and non-thermal arc plasma (NTAP), published in 2021, are especially noteworthy. The first paper [28] investigated a classical GA plasma, which has the major drawback of only sending a fraction of the total gas feed through the arc plasma [34]. Later, the same reactor was supplemented with a catalyst positioned downstream from the plasma, which reduced the EC (to 384 kJ/mol) and improved NH_3 conversion (to 70 %) [30]. However, the feedstock consisted of NH_3 diluted by N_2, which makes performance evaluation with most other plasma-based NH_3 cracking reactors less straightforward. The second paper [29] demonstrated highly efficient NH_3 decomposition on a large scale in an NTAP, with an EC as low as 157 kJ/mol when combined with a catalyst. However, this EC was still about 2.5 times higher than commercial thermo-catalytic NH_3 cracking (reaching 65 kJ/mol [6]; see above), and the conversion achieved in the plasma reactor was almost five times lower (20 % vs up to 95 %) [29,35]. The limited number of studies on the use of warm plasmas for NH_3 cracking into H_2 indicates that additional research is necessary to explore their full potential for this application.

Therefore, in this paper, we investigate the feasibility of plasma-based NH_3 cracking for green H_2 production. We will evaluate various warm plasmas for NH_3 cracking under a wide range of power and flow rate conditions. The aim is to compare the NH_3 conversion, EC, and H_2 production rates to reveal which are the best conditions and compare them with existing plasma-based NH_3 cracking and thermo-catalytic cracking. In addition, we want to obtain more insight into the underlying mechanisms of plasma-based NH_3 cracking in these warm plasmas.

2. Experimental setup

All our experiments in the various plasma reactors were conducted with pure NH_3, and the experimental system is illustrated in Fig. 1. The experimental setup consists of a gas supply system, a plasma system, and an analytics system. All parts of the experimental setup in direct contact with NH_3 were made from materials resistant to NH_3 and H_2.

All gas connections in the experimental setup were made using 1/4 in. PFA tubing and Swagelok 1/4 in. fittings. NH_3 (≈99.96 %, Air Liquide) was supplied into the system from 10 L gas cylinders using a Brooks SLA5850 mass flow controller (MFC). All mass flow rates were converted into a volumetric flow rate represented by normal litres per minute (Ln/min), with normal conditions defined as the temperature of 0 °C and pressure of 1 atm. Due to the low NH_3 vapour pressure at gas–liquid equilibrium at room temperature, two gas cylinders had to be used in parallel to maintain the NH_3 flow rates above 10 Ln/min without freezing the NH_3 gas cylinders. The flows from both NH_3 gas cylinders were mixed before entering the NH_3 MFC. N_2 (≈99.999 %, Air Liquide) was supplied using another Brooks SLA5850 MFC to flush the setup of NH_3 remains and decomposition products between the experiments. NH_3 was supplied at a set flow rate into each plasma reactor. The gas pressure at the outlet of the plasma reactor was monitored by a Wika DG-10-S pressure gauge. The system was fitted with a Swagelok SS-RL3S4-EP low-pressure proportional relief valve set to 180 kPa for overpressure protection.

The plasma system comprised a plasma reactor, a power supply, a ballast resistance if needed, and a watt meter for measuring power consumed from the mains. Four different warm plasma reactors were evaluated for their NH_3 decomposition performance: a rotating gliding arc (RGA), an atmospheric pressure glow discharge (APGD), a gliding arc plasmatron (GAP), and a pin-to-pin (P2P) arc discharge. We used the same gas supply and analytics systems for all plasma reactors.

The RGA, APGD and P2P reactors were powered by current-controlled direct current (DC) power supplies connected to the 3-phase power, each with a ballast resistor with a nominal resistance selected to stabilise the plasma (see Table 2). We used different power supplies, depending on the requirements of each specific plasma reactor,

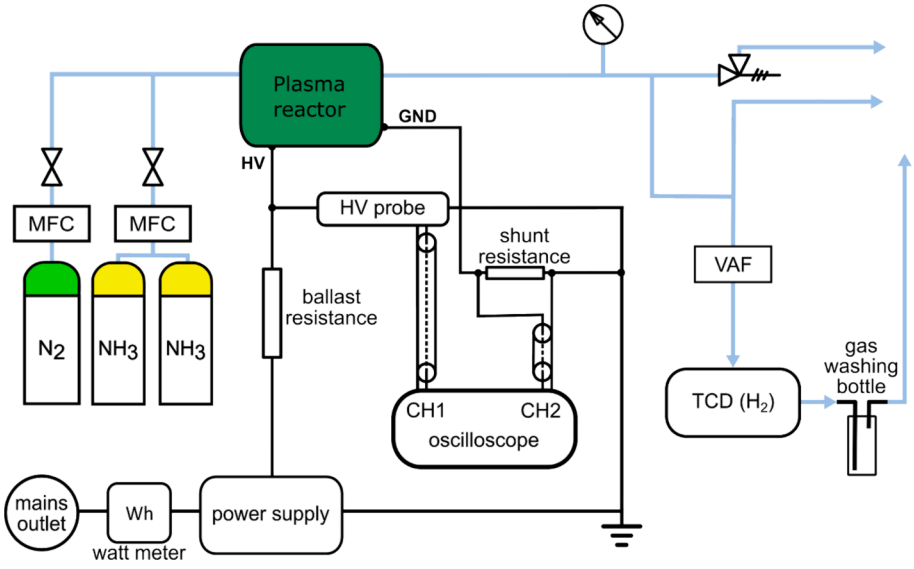

Fig. 1. Schematic overview of the experimental setup.

Table 2
Plasma system components for the investigated plasma reactors.

Plasma reactor	Power supply	Ballast resistance (kΩ)	Oscilloscope	Watt meter (mains power consumption)
RGA	Topower Tn-XX02	50	Tektronix TDS 2012C	Chauvin Arnoux Memo TD80
APGD	Technix SR30kV-1.2 kW	100	Tektronix TDS 2012C	Chauvin Arnoux Memo TD80
GAP	AFS G10P	None	Keysight DSO-X 1102G	Voltcraft Energy Check 3000
P2P	Technix SR12kV-10 kW	25	Rohde & Schwarz RTB 2004	Chauvin Arnoux Memo TD80

i.e., Topower Tn-XX02, Technix SR12kV-10 kW, and Technix SR30kV-1.2 kW, respectively (see Table 2). A Chauvin Arnoux Memo TD80 watt meter was used to monitor the power consumed by the whole plasma system. The methodology for measurement of the plasma power is described in section 3. Due to the loss of energy on the ballast resistors, the plug-to-plasma efficiency (ratio between plasma power and power consumed from the mains) of the RGA, APGD, and P2P systems was about 50 %. The GAP reactor was operated with the AFS G10P AC power supply connected to the residential power, which worked at 28 kHz and did not need a ballast resistor for stabilisation. The power consumption of the GAP plasma system was monitored with the help of a Voltcraft Energy Check 3000 W meter, and its plug-to-plasma efficiency was around 85 %.

Schematic diagrams of the investigated reactors are shown in Fig. 2. All investigated reactors were developed at the PLASMANT research group (University of Antwerp, Antwerp, Belgium) and used to study a variety of plasma-assisted gas conversion applications. The inlet of each reactor was connected to the gas supply system, while its outlet was connected to a volume leading to the gas analytics system. All reactors used the same gas supply and analytics systems and could be easily switched by disconnecting their inlet and outlet from the gas lines, taking them out and plugging in another reactor.

The RGA plasma reactor consists of an internal high-voltage (HV) electrode and a grounded (GND) electrode, which is also the reactor body. The HV electrode is a modified spark plug (NGK BP6ES) without a ground pin. The reactor body has a cone shape with the largest diameter of 13 mm and is connected to a cylindrical outlet 4 mm in diameter. The reactor body is 38 mm long. The electrodes are electrically isolated from each other by the ceramic body of the spark plug. The shortest inter-electrode distance in the reactor is 4 mm. The reactor outlet opens into the stainless-steel cylinder, providing a gas line connection out of the RGA reactor. More details of this reactor design can be found in [36].

The body of the APGD plasma reactor consists of a 300 mm long quartz tube with an internal diameter of 45 mm, which is connected on one end to the outlet gas line. On the other end, it is connected to a smaller quartz tube, 100 mm long, with a diameter of 10 mm, which contains a stainless steel HV grooved pin electrode with a diameter of 5 mm. The pin electrode is confined to the ceramic tube with an internal diameter of 5 mm. The feed gas enters the reactor through the smaller quartz tube and flows along the grooves of the pin electrode that act as gas channels. The ceramic tube that confines the pin electrode is in contact with a grounded plate mounted on three metal pins inside the main quartz tube. The movement of the pin electrode can adjust the inter-electrode distance. More details of this reactor design can be found in [37,38].

In the GAP reactor, the feed flow enters the reactor through a tangential inlet, creating a vortex flow. When the reactor outlet (which acts as a grounded electrode) has a smaller opening diameter than the reactor body (which acts as the HV electrode), the gas first moves towards the end of the reactor body in an outer forward vortex before it moves downward in a smaller inner reverse vortex and leaves the reactor through the outlet. An arc is ignited between the electrodes and is stabilised at the central axis of the reactor by the reverse vortex flow (RVF), which, in the ideal case, is forced to go through the plasma to reach the reactor outlet. More details of this reactor design can be found in [39,40].

Finally, the P2P reactor body consists of a quartz tube with an external diameter of 20 mm and an internal diameter of 16 mm. A stainless-steel pin inside a ceramic tube is inserted into each side of the quartz tube. The pins have 30 mm long cylindrical tungsten tips screwed on top of each of them, which serve as the electrodes. The side of the reactor with the HV electrode is connected to a swirler that supplies feed gas into the quartz tube, creating a forward vortex flow (FVF). The side of the reactor with the grounded electrode is connected to the gas outlet line. The inter-electrode distance in the reactor can be regulated by

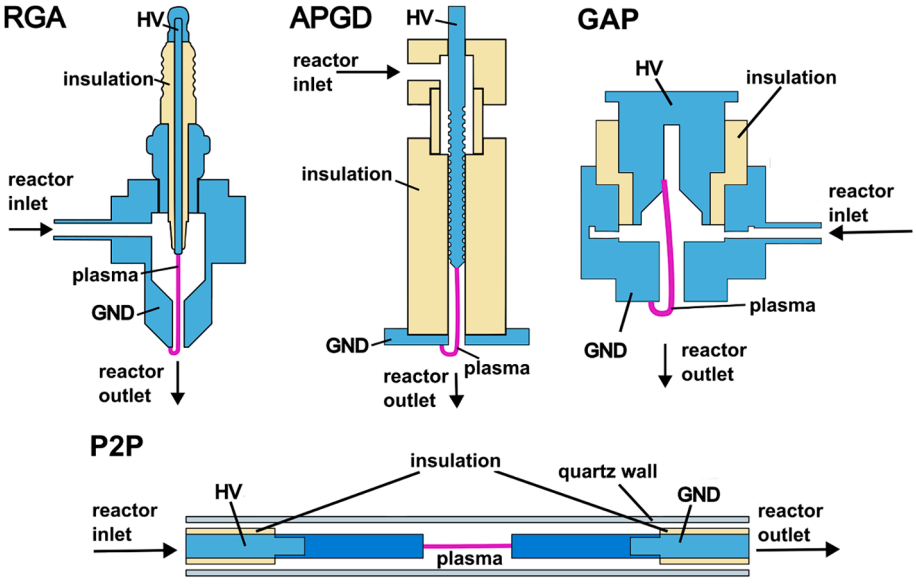

Fig. 2. Schematic diagrams of the four different plasma reactors: rotating gliding arc (RGA), atmospheric pressure glow discharge (APGD), gliding arc plasmatron (GAP), and pin-to-pin arc discharge (P2P). Each reactor's inlet and outlet, the high-voltage (HV) and grounded (GND) electrodes, insulation, and the plasma region are indicated.

moving the electrodes along the axis of the quartz tube. More details of this reactor design can be found in [41].

Each plasma reactor has different experimental parameters, such as flow rate and plasma power, allowing us to evaluate the NH_3 cracking performance in a wide range of conditions. A unifying condition between different reactors is the specific energy input (SEI) per unit of NH_3 introduced into the reactor. The specific reactor conditions are listed in Table 3.

Besides the feed flow rate, plasma power, and corresponding SEI range, Table 3 also includes the reactor volume for each reactor. Furthermore, the plasma itself is typically concentrated in the centre of the reactor and does not necessarily fill the entire reactor volume. Therefore, we also added approximate estimates of the volume of the plasma zone for each reactor. Indeed, the plasma zone, together with the gas flow rate, might give a first indication of the residence time of the gas inside the plasma, which is also important for determining the NH_3 conversion. From these values, we can estimate the residence time of NH_3 feed inside the plasma to be around 2–3 ms in the GAP reactor, 5–18 ms in the P2P reactor, 18 ms in the RGA reactor, and 8–48 ms in the APGD reactor. However, this estimation does not account for complex and possibly turbulent flow dynamics, which are taking place inside the plasma reactors due to vortex flows. Additionally, the NH_3 cracking takes place not only inside the plasma core but also in the hot zone around the plasma, which is hard to estimate without knowing the temperature profile inside each plasma reactor. Therefore, it is not possible at this stage to estimate the real residence time and, thus, its impact on the conversion. This would require input from fully coupled 3D (or 2D axisymmetric) modelling of the reactors, incorporating gas flow, plasma dynamics and chemistry, but such models have not yet been developed to the required level.

3. Measurement methods

The average power supplied to each of the plasma reactors (P_{plasma}) was calculated as an average between the average instantaneous powers of m recorded waveforms, containing the instantaneous discharge current $I_m(k)$ and voltage $U_m(k)$, each with n samples of current and voltage per waveform:

$$P_{plasma} = \frac{1}{m}\sum_{i=1}^{m}\left(\frac{1}{n}\sum_{k=1}^{n} U_i(k)\cdot I_i(k)\right) \quad (1)$$

The discharge current and voltage waveforms were recorded via Tektronix TDS 2012C, Keysight DSO-X 1102G, or Rohde & Schwarz RTB 2004 oscilloscopes. The discharge voltage was measured using a high-voltage probe (Pintek HVP-39pro). The discharge current was determined by measuring the voltage drop on a 10 Ω shunt resistance. In our research, the power was averaged over $m = 10$ waveforms for each measurement point. For the power calculations for the AC discharge in the GAP reactor, the waveforms were recorded at a horizontal scale that was picked to allow the capture of at least 20 AC periods and trimmed to include only an integer number of periods.

The outlet gas line was split into an extraction line and an analytics line leading to a Swagelok® VAF-G2-01 M-1–0-G variable area flow meter, a gas analyser, and a 500 mL gas washing bottle, followed by another extraction line. The outlet gas composition was analysed for its H_2 content using a Rosemount™ X-Stream Enhanced general-purpose gas analyser equipped with a thermal conductivity detector (TCD) capable of measuring the H_2 concentration from 0 % to 100 % with an accuracy of 0.5 %. Due to the non-selective nature of TCD measurements and the cross-sensitivity of a TCD to gases besides H_2, the gas analyser was calibrated with a range of mixtures containing NH_3, H_2, and N_2, simulating the decomposition products at different NH_3 conversions. The resulting calibration curve, illustrated in the Supporting Information (SI, section S1), was used to calculate the H_2 concentration in the NH_3 decomposition products. The H_2 concentration was recorded after its fluctuations measured by the gas analyser were less than 1 % relative to its value for more than 2 min. The resulting H_2 concentration was measured by averaging the concentration data recorded for 1 min.

The gas washing bottle set on the analytics line was used to test each setup for the presence of hydrazine (N_2H_4) in the decomposition products. Hydrazine was collected by passing a set flow rate of the decomposition products for a set time through a gas washing bottle filled with 250 mL of deionised water. 1 mL of the hydrazine-containing solution was mixed with 100 μL of the Hy-1 reagent from the Spectroquant Hydrazine Test Kit and incubated for 10 min. The hydrazine content in the resulting solution was measured via spectrophotometry using a UV–Vis Thermo Fischer Genesys 6 spectrophotometer with Hellma quartz cuvettes with a 10 mm path length. The hydrazine content was determined using calibration for the absorbance measured at the peak maximum of 458 nm. More details about this measurement can be found in SI, section S.2.

The quartz wall of the P2P reactor allowed for the capture of its emission spectrum, which was used to estimate the plasma temperature in the arc discharge. The temperature was calculated based on the relative intensity measurements of the spectral lines in the rotational structure of the second positive system of nitrogen ($N_2\ C^3\Pi_u \rightarrow B^3\Pi_g$) in the 350–390 nm range, which was recorded using an Avantes AvaSpec-3048 high-resolution spectrometer. The temperature was obtained by fitting the experimental data to simulated spectra using SpecAir software [42].

Due to the differences between the plasma reactors, the key common parameter describing the operating conditions is the SEI per mole of NH_3:

$$SEI\left(\frac{kJ}{mol}\right) = \frac{P_{plasma}(W)\cdot 60\left(\frac{s}{\min}\right)}{1000\left(\frac{W}{kW}\right)\cdot Q^{in}_{NH_3}\left(\frac{Ln}{\min}\right)}\cdot V_m\left(\frac{Ln}{mol}\right) \quad (2)$$

where $Q^{in}_{NH_3}$ is the mass flow rate of NH_3 in the feed into each reactor, and V_m is the molar volume of the feed gas, for which we use 22.4 Ln/mol as these are the units used by our MFC to represent the mass flow rate of gas.

The performance of each plasma reactor was evaluated based on two parameters: NH_3 conversion (X_{NH_3}) and EC of NH_3 decomposition. H_2 production rate is another interesting parameter that will be compared later in this paper. The NH_3 conversion was calculated from the H_2 concentration in the decomposition products based on the assumption that NH_3 decomposes to a 3:1 mixture of H_2 and N_2 with a statistically insignificant quantity of other byproducts. This assumption was confirmed multiple times in the literature [9,10,15,23] and by our experiments, as explained in the SI, section S.2.

We must account for the gas expansion during NH_3 decomposition because 2 mol of NH_3 decompose into 3 mol of H_2 and 1 mol of N_2. Therefore, the NH_3 conversion should be calculated as:

$$X_{NH_3} = \frac{y^{in}_{NH_3} - \alpha\cdot y^{out}_{NH_3}}{y^{in}_{NH_3}} = 1 - \alpha\cdot y^{out}_{NH_3} = 1 - \frac{(1 - X_{NH_3}) + \frac{3}{2}X_{NH_3} + \frac{1}{2}X_{NH_3}}{1}\cdot y^{out}_{NH_3}$$
$$= 1 - (1 + X_{NH_3})\cdot y^{out}_{NH_3} \quad (3)$$

Table 3
Experimental conditions for the four different plasma reactors.

Plasma reactor	NH_3 feed flow rate (Ln/min)	Plasma power (W)	SEI range (per NH_3) (kJ/mol)	Approximate reactor volume (mL)	Approximate plasma zone volume (mL)
RGA	1	70–350	104–291	4.7	0.3
APGD	1–3	55–235	30–300	1–1.4	0.4–0.8
GAP	10–20	220–910	30–120	7.3	0.5
P2P	10–20	60–1200	7–130	15.1–19.1	1.5–2.5

where $y^{in}_{NH_3}$ is the fraction of NH_3 in the feed (our feed contains only NH_3, so $y^{in}_{NH_3} = 1$), $y^{out}_{NH_3}$ is the fraction of NH_3 in the decomposition products, and α is the gas expansion coefficient calculated according to the methodology described in [43]. By rearranging Eq. (3) to extract the conversion, we get:

$$X_{NH_3} = \frac{1 - y^{out}_{NH_3}}{1 + y^{out}_{NH_3}} \tag{4}$$

The EC of NH_3 decomposition is calculated from the SEI and the NH_3 conversion:

$$EC\left(\frac{kJ}{mol}\right) = \frac{SEI\left(\frac{kJ}{mol}\right)}{X_{NH_3}} \tag{5}$$

Finally, the H_2 production rate equals the flow rate of H_2 at the reactor outlet ($Q^{out}_{H_2}$) and is calculated from $Q^{in}_{NH_3}$, X_{NH_3} and taking into account that 2 mol of NH_3 decompose into 3 mol of H_2 via Eq. (6):

$$Q^{out}_{H_2} = Q^{in}_{NH_3} \cdot X_{NH_3} \cdot \frac{3}{2} \tag{6}$$

Each parameter is obtained as an average of three repeat measurements of plasma power and NH_3 conversion at each investigated operating condition. The errors reported in this work are equal to the standard deviations calculated from the values for the above-mentioned repeat measurements.

4. Results and discussion

We performed NH_3 cracking in the four different plasma reactors described above for different feed flow rates and SEI values. While the performance of each individual reactor is interesting, our goal was to compare and contrast them against each other and the state-of-the-art, taken from the literature. By studying several (somewhat similar) reactors at the same time, we can gain additional insight into the underlying mechanisms of plasma-assisted NH_3 cracking and identify possible limitations of the process.

4.1. RGA plasma reactor

The results of NH_3 conversion and EC in the RGA plasma reactor are plotted in Fig. 3. All measurements were conducted at a 1 Ln/min feed flow rate.

Based on the plasma power introduced in the RGA reactor (i.e., 70–350 W), the SEI ranges between 100 and 300 kJ/mol. The NH_3 conversion rises almost linearly with the SEI. The RGA reactor achieves the highest conversion out of all tested plasma reactors: 83 %, with an EC of 360 kJ/mol at an SEI of 290 kJ/mol. The lowest EC of NH_3 decomposition achieved in the RGA reactor is 320 kJ/mol, with an NH_3 conversion of 49 %. The EC of decomposition in the RGA reactor shows little dependence on the SEI: on average, it stays between 300 and 400 kJ/mol. This behaviour follows directly from Eq. (5) because the rise in NH_3 conversion is proportional to the increase of SEI.

The presented data comes with the caveat of high measurement errors, limiting the reliability of the results. The error spans from the changes in the discharge electrodes during the reactor operation. During the experiments, the HV electrode of the RGA reactor underwent significant erosion, potentially due to the critically high temperature of the electrode tip. As a result, the performance of the RGA plasma reactor during NH_3 decomposition was unstable, leading to large error margins when calculating the average NH_3 conversion and EC. We believe this explains the unexpected trend (noticeable deflection) in NH_3 conversion and EC observed at SEI above 200 kJ/mol in Fig. 3, and there is no physical reason for this trend. The observed changes in electrode configuration and the instability led to the lack of repeatability in the experimental results. As such, the presented results are more indicative of the potential of the RGA reactor for NH_3 decomposition than of its optimal performance.

In its original configuration, the RGA reactor achieves a high NH_3 conversion due to its ability to reach a high SEI. The reactor has the potential to be highly performant for NH_3 decomposition, but it is hampered by the insufficient cooling of the HV electrode. Further redesigns and adjustments are needed to fully exploit the potential of the RGA plasma reactor for NH_3 decomposition. This can be done by replacing the HV electrode with a material with a higher melting point, such as tungsten, or by the addition of electrode cooling. Both options require a complete redesign of the HV part of our RGA plasma reactor, which was beyond the scope of this study.

4.2. APGD plasma reactor

Fig. 4 illustrates the results of NH_3 conversion (top) and EC (bottom) for the APGD plasma reactor at different feed flow rates (1, 1.5, 2, 2.5, and 3 Ln/min) and different inter-electrode distances (20, 30, and 40 mm). A larger inter-electrode distance requires a higher applied voltage at the same discharge current, which results in a higher power and, consequently, a higher SEI at the same feed flow rate. Indeed, the maximum SEI, achievable for 1 Ln/min feed flow rate with the available power supply and ballast resistor, rises by about a factor of two, from 152 kJ/mol at 20 mm to 287 kJ/mol at 40 mm. As a result, the NH_3 conversion also rises, although less than a factor two, i.e., from 48 % at 20 mm to 78 % at 40 mm, and therefore, the EC slightly rises, from 319 kJ/mol at 20 mm to 367 kJ/mol at 40 mm inter-electrode distance. A comparison between the NH_3 conversions at the same feed flow rate and the same SEI but at different inter-electrode distances shows that at longer inter-electrode distances the conversion slightly decreases, indicating the loss of NH_3 decomposition efficiency. This can be attributed to the decrease of power density at longer inter-electrode distances when maintaining a constant SEI at the same feed flow rate (and thus constant power) due to the increase of plasma volume. This could reduce the feed gas temperature during the cracking process, resulting in a lower conversion. However, this assumption is only a hypothesis, which we plan

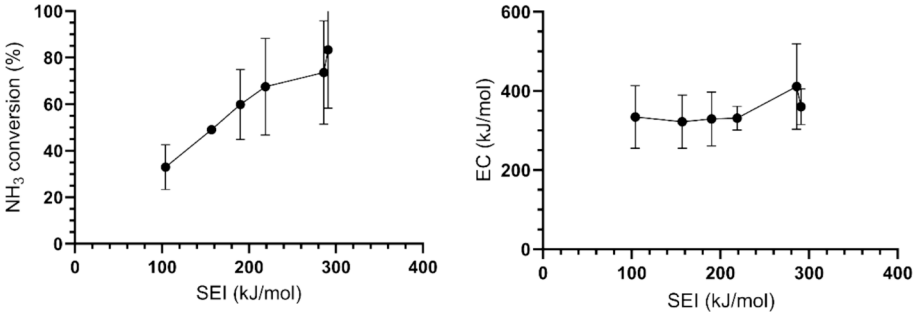

Fig. 3. NH_3 conversion (left) and EC (right) in the RGA plasma reactor, as a function of SEI per mole of NH_3 feed. Feed flow rate – 1 Ln/min.

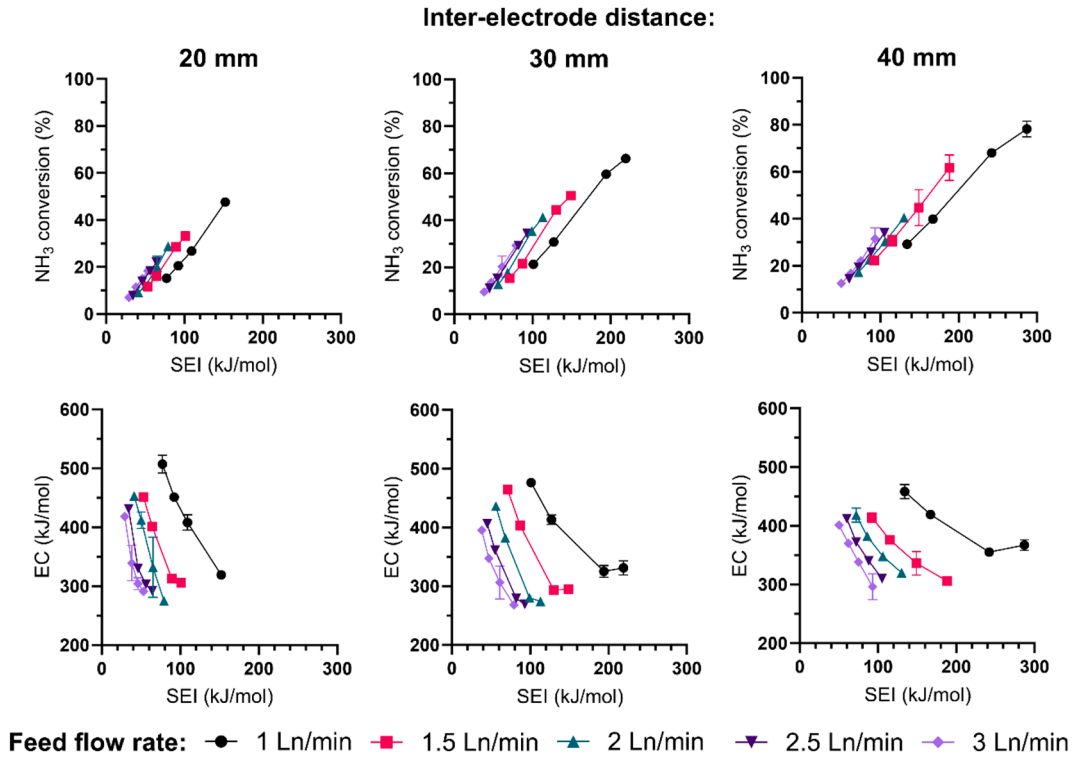

Fig. 4. NH_3 conversion (top) and EC (bottom) in the APGD plasma reactor, as a function of SEI per mole of NH_3 feed, for different feed flow rates and inter-electrode distances.

to test in our future work using computer modelling.

Overall, the NH_3 conversion in the APGD plasma reactor rises faster than the rise in SEI. Consequently, the EC of NH_3 conversion significantly drops upon higher SEI (cf. Eq. (5)). This behaviour differs from that in the RGA plasma reactor, where the EC was more or less constant. This indicates that a higher SEI is advantageous in the APGD reactor because it yields a higher NH_3 conversion and lower EC. However, the increase in NH_3 conversion slows down at the highest conversion values (cf. 1 Ln/min feed flow rate and inter-electrode distance of 30 and 40 mm), which explains the slight rise in EC. This indicates that the APGD reactor will require progressively higher SEI to achieve complete NH_3 conversion. The highest NH_3 conversion of 78 % was achieved at an EC of 367 kJ/mol for an SEI of 287 kJ/mol, a feed flow rate of 1 Ln/min, and an inter-electrode distance of 40 mm. When the SEI of the system is kept constant, the feed flow rate directly impacts the NH_3 conversion, with a higher flow rate corresponding to a higher conversion. This can be explained by the fact that the plasma power should rise correspondingly at a higher flow rate when the SEI is kept constant. Hence, the higher power has more impact on the NH_3 conversion than the higher flow rate (or shorter residence time). Nevertheless, the conversion difference between different flow rates decreases at higher flow rates and may become negligible for feed flow rates exceeding 3 Ln/min.

The lowest EC of NH_3 decomposition in the APGD plasma reactor is 269 kJ/mol, corresponding to 34 % NH_3 conversion at 2.5 Ln/min feed flow rate and 30 mm interelectrode distance. Of all tested plasma reactors, the APGD reactor exhibits the most pronounced drop in EC upon rising SEI, from 450 – 500 kJ/mol to 270 – 300 kJ/mol. As with the NH_3 conversion, the EC is improved by applying a higher feed flow rate while maintaining the same SEI.

Compared with the RGA reactor, the APGD reactor reaches similar NH_3 conversion at similar SEI values. We could apply higher SEI values in the RGA and APGD reactors than in the GAP and P2P reactors (see following sections) because they operate at slightly lower plasma power but significantly lower feed flow rates (see Table 3), which explains their high NH_3 conversion. Additionally, at the same feed flow rate, the EC of NH_3 decomposition in both APGD and RGA reactors is very close. Increasing the feed flow rate and reducing the inter-electrode distance benefit the APGD reactor performance at the same SEI. While the exact reason for the conversion improvement is unclear, both actions reduce the residence time of the feed gas inside the plasma reactor and potentially increase the feed gas temperature during cracking due to a higher power density inside the plasma. Last but not least, the APGD reactor showed no signs of erosion or overheating after the experiments, which is a significant advantage compared to the RGA reactor.

4.3. GAP plasma reactor

The NH_3 conversion and EC of NH_3 decomposition in the GAP plasma reactor are plotted as a function of SEI in Fig. 5 for five different feed flow rates (10, 12.5, 15, 17.5, and 20 Ln/min). The power supply output power was varied between 250 and 1000 W, which resulted in a plasma power between 220 and 910 W and an SEI between 30 and 60 kJ/mol for all feed flow rates. In addition, we also performed experiments at higher SEI (60–120 kJ/mol), but the maximum power supply output only made this possible at the lowest feed flow rate of 10 Ln/min.

The GAP plasma reactor showed higher stability for NH_3 conversion than the RGA and APGD reactors, which can be observed from the smaller error bars in the NH_3 conversion and EC data. Within the tested range of SEI, the NH_3 conversion shows a linear increase with rising SEI. The highest NH_3 conversion is 51 % with EC of 235 kJ/mol, achieved at 10 Ln/min feed flow rate and SEI of 120 kJ/mol. In general, although the maximum SEI value reached in the GAP reactor is lower than what could be obtained in the RGA and APGD reactor, the GAP reactor reaches a higher NH_3 conversion than the RGA and GAP reactor at the same SEI, in most cases outperforming them by up to 10 %. The observed difference between NH_3 conversion values at the tested feed flow rates is small, indicating that SEI is a major factor determining NH_3 conversion in the GAP reactor.

Upon rising SEI in the GAP reactor, the EC of NH_3 decomposition drops from about 260 to 220 kJ/mol at 10 Ln/min and more moderately

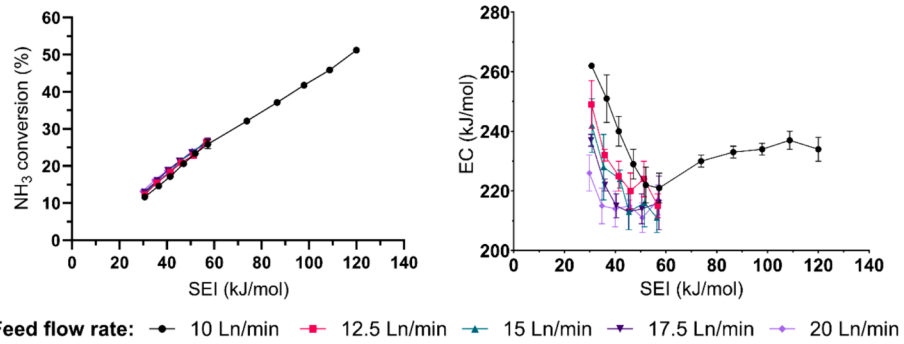

Fig. 5. NH_3 conversion (left) and EC (right) in the GAP plasma reactor, as a function of SEI per mole of NH_3 feed, for different feed flow rates.

from 225 to 215 kJ/mol at 20 Ln/min. This can be explained by the fact that the NH_3 conversion rises slightly faster than the SEI, especially at 10 Ln/min (cf. Eq. (5)). However, starting at an SEI of 50 kJ/mol, the EC remains constant in the 210–230 kJ/mol range, depending on the feed flow rate. The lowest EC achieved in the GAP reactor is 210 kJ/mol with an NH_3 conversion of 27 % at 15 Ln/min feed flow rate and 56 kJ/mol SEI. This value is 60 kJ/mol and 110 kJ/mol lower than the lowest values observed in the APGD and RGA plasma reactor, respectively.

Finally, as mentioned above, the GAP reactor exhibits stable NH_3 decomposition performance at all conditions investigated. It shows several advantages over the RGA and APGD reactors: fewer fluctuations in the NH_3 conversion, a lower EC, and higher operating feed flow rates, which yield higher H_2 production rates, as will be discussed in section 4.5. However, during the experiments at SEI values higher than 60 kJ/mol, the reactor body reached temperatures exceeding 327 °C. This is evidenced by the melting and slight deformation of the PTFE isolator placed between the GAP electrodes. This indicates that the GAP reactor has to be equipped with either additional electrode cooling or a ceramic isolator if we want to increase the SEI to enhance the NH_3 conversion further. This will be the subject of future work.

4.4. P2P arc plasma reactor

Fig. 6 illustrates the NH_3 conversion and EC data for the P2P low-current arc plasma reactor at four feed flow rates (5, 10, 15, and 20 Ln/min). The inter-electrode distance between both pins was set to 30 mm. The SEI in the P2P reactor was regulated via the discharge current, which was between 20 and 50 mA for all feed flow rates. Additional measurements were done at 130 mA for 10 and 20 Ln/min, and at 150 and 170 mA for 20 Ln/min. The SEI range was limited to under 80 kJ/mol due to excessive heating and melting of the inner part of the plasma reactor quartz wall (melting point at 1670 °C) at higher SEI values.

The NH_3 conversion dependence on the SEI in the P2P reactor resembles the behaviour in the GAP reactor, with an almost linear conversion increase with SEI, similar conversion values and only limited dependence on the feed flow rate. The highest NH_3 conversion in the P2P reactor reaches 28 % with an EC of 235 kJ/mol at 10 Ln/min feed flow rate and an SEI of 66 kJ/mol.

The EC of NH_3 decomposition in the P2P reactor is at a minimum when the SEI is below 30 kJ/mol for all feed flow rates investigated. The minimum at 20 Ln/min corresponds to the lowest EC of NH_3 decomposition in the P2P reactor and all the other plasma reactors investigated, reaching 146 kJ/mol at an SEI of 11 kJ/mol. However, the NH_3 conversion is limited to only 8 % at this low SEI. The EC of NH_3 decomposition in the P2P reactor increases upon raising the SEI. Thus, it behaves differently from the other plasma reactors, where the EC stays constant or even drops (APGD and GAP at low SEI) upon rising SEI. To investigate whether a further increase of SEI will further enhance the EC, we performed additional experiments at 20 Ln/min feed flow rate, an inter-electrode distance of 50 mm, and higher discharge currents of 130, 150, and 170 mA. The larger inter-electrode distance led to a higher applied voltage at the same current values, increasing the SEI while maintaining the temperature of the reactor components low enough to avoid thermal damage. The results of these additional experiments are plotted in Fig. 7.

Operating at higher SEI enhances the NH_3 conversion, achieving a new maximum of 36 % with an EC of 225 kJ/mol at 20 Ln/min feed flow rate and SEI of 80 kJ/mol. The obtained data confirms that increasing the SEI in the P2P reactor leads to a rise in both the NH_3 conversion and EC. This is because the NH_3 conversion rises slightly slower than the SEI (cf. Eq. (5)). As a result, using the P2P arc plasma reactor for NH_3 decomposition may be limited by the necessity to choose between a high conversion (operating at high SEI) or a low EC (operating at low SEI), depending on the needs of a particular application. On the other hand, the rise in EC seems more moderate (especially in the higher SEI range) than the rise in NH_3 conversion. Hence, operating at a higher SEI might be beneficial, yielding higher conversion at only a slightly higher EC. However, operating at higher SEI was currently not possible in the P2P reactor due to thermal damage.

As mentioned in section 3, the quartz tube of the P2P reactor allows

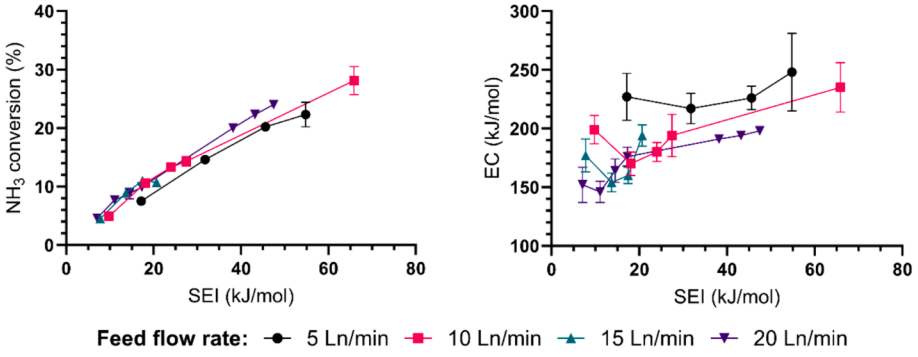

Fig. 6. NH_3 conversion (left) and EC (right) in the P2P arc plasma reactor, as a function of SEI per mole of NH_3 feed at different feed flow rates.

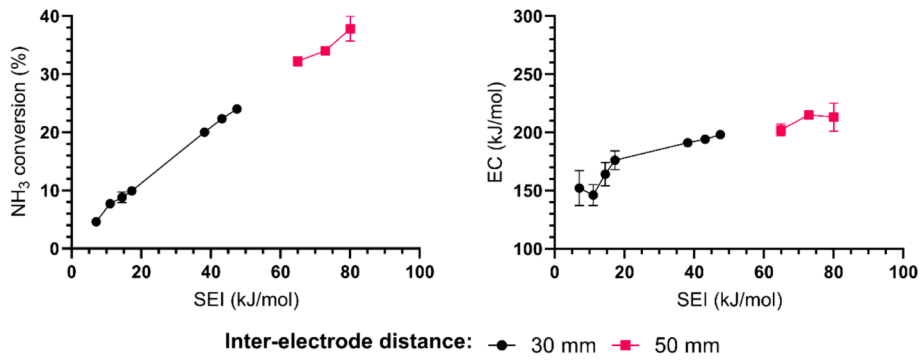

Fig. 7. NH_3 conversion (left) and EC (right) in the P2P arc plasma reactor, as a function of SEI per mole of NH_3 feed at two different inter-electrode distances. Feed flow rate – 20 Ln/min.

OES measurements to obtain the rotational temperature inside the plasma. In warm plasma, the rotational temperature is a good measure of the gas temperature. When operating at a feed flow rate of 20 Ln/min and SEI of 68.9 kJ/mol, we obtained the best fit of the OES spectrum for a rotational temperature of 4000 ± 500 K inside the core of the arc plasma channel (see section S3 in SI for the fitted spectrum). We could not obtain reliable values at lower SEI due to a very low signal-to-noise ratio in the measured emission spectra, which may indicate a decrease in temperature. The measured temperature of 4000 K indicates that the NH_3 conversion will proceed mainly by thermal chemistry, as was demonstrated in [24], although non-thermal chemistry cannot be conclusively ruled out. A more detailed investigation of the contribution of thermal vs non-thermal chemistry requires complex computer simulations, which is out of the scope of this work.

In conclusion, the P2P arc plasma reactor exhibits the lowest EC of NH_3 decomposition among all plasma reactors investigated in this study. However, the simultaneous increase in NH_3 conversion and EC poses a limitation that is absent for the other reactors, although this rise in EC is limited in the higher SEI range. In addition, the P2P discharge in NH_3 posed the highest risk to the reactor integrity due to high heat transfer from plasma to reactor components and the corresponding thermal damage.

4.5. Comparison between the reactors

Based on our extensive study, we can see that the different reactor configurations exhibit different performances and trends in terms of NH_3 conversion and EC within the given SEI range. Fig. 8 compares the NH_3 conversion, EC, and H_2 production rates of the four different reactors at their best-performing flow rate: 1 Ln/min for the RGA reactor, 3 Ln/min for the APGD reactor, and 20 Ln/min for the GAP and P2P reactors. These NH_3 flow rates correspond to the shortest estimated residence times of gas inside the plasma for each reactor. Such behaviour may indicate that at longer residence times the NH_3 feed is overheated inside the plasma at the investigated reactor conditions, leading to a loss of efficiency. In addition, the GAP features data at 10 Ln/min as this was the flow rate at which we could perform experiments at higher SEI (see section 4.3), allowing us to compare the performance over a somewhat wider SEI range.

We managed to operate the APGD, GAP and P2P reactors in a similar range of SEI, which allows for a more direct comparison between these reactors. The P2P and GAP show very similar conversions, slightly exceeding that of the APGD reactor at the same SEI. The NH_3 conversion of the RGA reactor is higher, but it suffers from much higher variability between the experimental repeats. The higher NH_3 conversion in the RGA reactor stems from operation at a higher SEI than the other reactors. By extrapolating trends of the P2P, GAP, and APGD NH_3 conversion plots into the higher SEI range, we can expect that the P2P and GAP reactors will reach a higher conversion than the RGA and APGD.

The EC obtained in the four reactors separates them into two groups: the P2P and GAP reactors with a very close EC at approximately 200 kJ/mol (or lower for the P2P reactor) and the APGD and RGA reactors with EC around 300 kJ/mol. The P2P reactor shows the best EC of all investigated reactors (down to 146 kJ/mol) due to its operation at lower SEI, but for that same reason, it corresponds to the lowest NH_3 conversion.

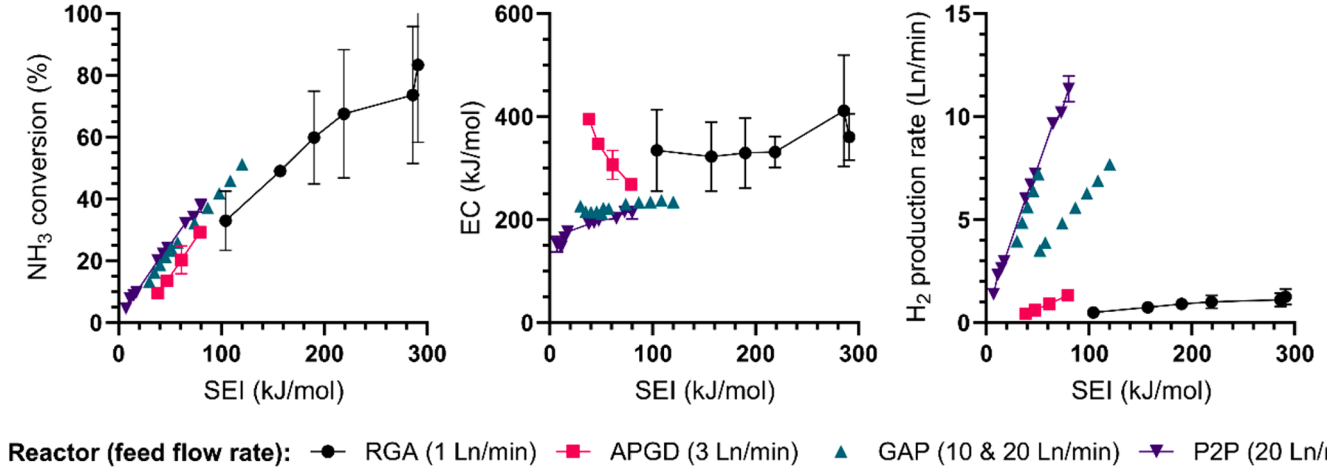

Fig. 8. NH_3 conversion (left), EC (middle), and H_2 production rate (right) in the investigated plasma reactors, as a function of SEI per mole of NH_3 feed. Each reactor is represented at its best-performing feed flow rate: 1 Ln/min for RGA, 3 Ln/min for APGD, 10 and 20 Ln/min for GAP, and 20 Ln/min for P2P. Data for the GAP is plotted for both 10 and 20 Ln/min to compare its performance over a wider SEI range.

Another striking difference in the EC data is the variety of the change of EC with SEI between the reactors. Indeed, it stays more or less constant in the RGA and GAP reactor (at least for 20 Ln/min; at lower flow rates, the GAP shows a drop in EC upon rising SEI, followed by a slight rise above SEI=60 kJ/mol; see Fig. 5). In contrast, the P2P reactor exhibits a slightly upward EC trend with rising SEI, while the APGD shows a clear drop in EC. This behaviour is explained by the variation of NH_3 conversion upon SEI increase: if the NH_3 conversion rises faster than the SEI, it results in a drop in EC upon higher SEI, but if the rise in NH_3 conversion is slower than the rise in SEI, the EC rises upon higher SEI (cf. Eq. (5)).

The different EC behaviour and the different slope of the NH_3 conversion vs SEI of the four reactors point to some differences in the underlying mechanisms of conversion, even at a comparable SEI range. For the APGD, GAP, and P2P reactors, the SEI is very close, indicating that the energy input in the gas is the same. If this same energy input yields a similar electron temperature and gas temperature in the plasma, this would mean that the underlying chemistry of the conversion, either thermal or non-thermal, is the same. Therefore, there must be other reasons for the difference. This will be discussed in section 4.7 below.

Overall, when comparing the four different plasma reactors, we see that the reactors with higher flow rates (P2P, GAP) perform better than those with lower flow rates (APGD, RGA) at the same SEI. Despite similar conversion in the P2P and GAP reactors, the P2P reactor manages to reach a lower minimum EC (146 kJ/mol) than the GAP (211 kJ/mol). Both reactors, however, produce excess heat during operation, which causes reactor damage and is wasted, potentially increasing the EC of cracking. Hence, they need modifications and adjustments, especially to expand their SEI operating range and further improve their EC.

In general, Fig. 8 suggests that all four reactors might show further performance improvements when operating at higher SEI. Indeed, the conversion rises with SEI, while the EC stays constant or even drops (for the APGD). Furthermore, the H_2 production rate rises dramatically (especially for the GAP and P2P reactors). Indeed, the H_2 production rate depends largely on the operating flow rate. The P2P and GAP reactor, working at 20 Ln/min, show by far the highest H_2 production rate due to their higher flow rate than the RGA and APGD (cf. right panel of Fig. 8). The maximum production rate achieved in our study is 11.3 Ln/min, namely for the P2P reactor operating at a flow rate of 20 Ln/min and SEI of 80 kJ/mol. Moreover, Fig. 8 suggests that it would rise further if we could apply a higher SEI (hence higher power, keeping a high flow rate).

However, expanding the reactors to higher SEI (or higher power) requires modifications to the reactor designs, including specific heat-resistant materials, to avoid thermal damage. This will be pursued in our future work.

4.6. Comparison with the state-of-the-art

To benchmark our results with existing literature, we compare in Fig. 9 the NH_3 conversion vs EC of our investigated plasma reactors with all data found in other works on plasma NH_3 cracking. The literature data presented in Fig. 9 comprises plasma-based decomposition of pure NH_3 with EC below 10 MJ/mol. Indeed, literature data with even higher EC (see Table 1 in the Introduction) or for diluted NH_3 mixtures are not interesting or relevant for comparison. Most studies reported in the literature were performed in cold plasma reactors, such as DBD reactors [8–20], DBD reactors with catalysts [8–10,12–16,18] with or without external heating, and DBD reactors with hydrogen membrane [12,19]. Studies involving warm plasma reactors for pure NH_3 cracking are much more scarce (see Table 1 in the Introduction) and only include an atmospheric pressure AC discharge [27], a GA plasma [28], and a non-thermal arc plasma (NTAP) [29]. Fig. 9 makes a distinction between cold plasmas (with and without catalyst) and warm plasmas (again with and without catalyst). Our reactors ("This work") also belong to the category of warm plasmas.

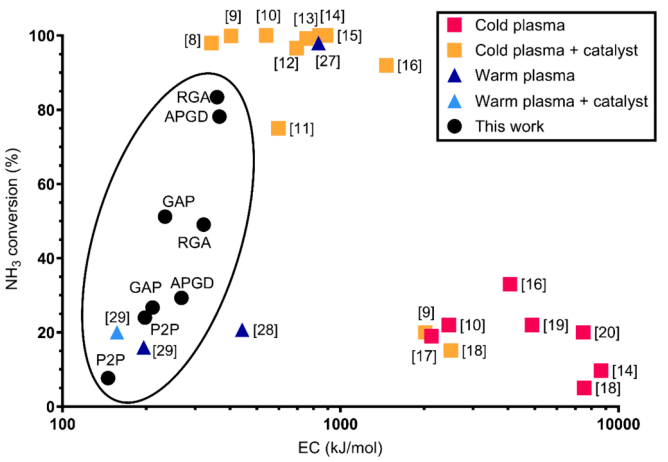

Fig. 9. NH_3 conversion, plotted as a function of EC, for our four investigated plasma reactors and compared with literature data (see corresponding references in Table 1 for the operating conditions of the literature reactors). The red squares correspond to cold plasmas (DBD), the orange squares are the same cold plasmas, but with catalyst, the dark blue triangles correspond to warm plasmas (AC, GA and NTAP), while the light blue triangle is NTAP with catalyst. Finally, the black data points, contained by the black oval, originate from our work (APGD, GAP, P2P and RGA). Note the logarithmic scale of the x-axis.

It is clear from Fig. 9 that cold (non-thermal) plasma reactors without catalysts exhibit very poor NH_3 decomposition performance, with NH_3 conversion typically around or below 20 %, and, especially, very high EC exceeding 2 MJ/mol. Note the logarithmic scale of the x-axis in Fig. 9. The performance of these reactors can be significantly improved by adding catalysts, such as Fe, Ni, Co, and Ru, inside the plasma, leading to a conversion close to 100 %, although the EC remains rather high (300–2000 kJ/mol). Moreover, even with added catalysts, an external heat source is often required to reduce the EC below 800 kJ/mol (cf. Table 1). For example, the lowest EC achieved in these cold plasma reactors was 345 kJ/mol, with 98 % NH_3 conversion at 0.04 Ln/min feed flow rate, applying a DBD reactor that was packed with Co/SiO_2 catalyst, using Co nanoparticles with 27 wt% metal loading, but also preheated to 380 °C [8]. This makes cold plasmas less appealing for NH_3 cracking, as they need to use the same catalysts as thermal catalysis at similar conditions but at much higher EC [35]. Compared to these cold plasma reactors, the warm plasma reactors investigated in our work exhibit significantly lower EC even without using any catalysts.

The performance characteristics of our plasma reactors are similar to those of the other warm plasma reactors reported in the literature: GA and NTAP. The lowest EC achieved in our GAP plasma reactor (211 kJ/mol) is only 5 % higher than the lowest EC of purely plasma-based NH_3 decomposition in the NTAP reactor (196 kJ/mol), while the NH_3 conversion obtained in our GAP reactor in this case is 67 % higher than in the NTAP [29] (i.e., 16 % in NTAP vs 27 % in GAP). The higher conversion in our GAP compared to the NTAP most likely originates from the higher SEI supplied to the GAP (i.e., 35 kJ/mol in the NTAP vs 55 kJ/mol in the GAP), which in our experiments has been shown to lead to increased NH_3 conversion. We see the same picture for our P2P reactor, which reaches 24 % conversion at an EC of 198 kJ/mol, hence 50 % higher than the NTAP (16 %) at the same EC (196 kJ/mol). Finally, our P2P reactor shows the lowest EC among all plasma-based systems for NH_3 decomposition reported up to now (146 kJ/mol), even below the NTAP plasma reactor combined with post-plasma catalysis (157 kJ/mol), albeit at a low NH_3 conversion.

When comparing the H_2 production rate, we see that most reactors in literature were operated at low flow rates, which severely hampers the amount of H_2 they could produce. In the cold (DBD) reactors, the highest H_2 production rate was 0.29 Ln/min (feed flow rate of 1 Ln/min) without catalysts [17] and 1.45 Ln/min (feed flow rate of 1 Ln/min)

with catalysts [12]. The highest H_2 production rate achieved in the literature for cracking of pure NH_3 was 9 Ln/min in the NTAP reactor operating at 30 Ln/min feed flow rate with post-plasma catalysis [29]. In our work, we exceeded this H_2 production rate with our P2P reactor at 20 Ln/min NH_3 flow rate, producing H_2 at a rate of 11.3 Ln/min.

Finally, when comparing our results with the best data reported in the literature for commercial thermo-catalytic NH_3 cracking (which reaches up to 95 % conversion at an EC of only 65 kJ/mol [6]), it is clear that plasma-based NH_3 cracking is not yet competitive. We need to further improve the cracking performance by employing smart reactor design, including modifications to allow reactor operation at higher SEI. On the other hand, our plasma reactors do not require expensive Ru-based catalysts that dominate the field of thermo-catalytic NH_3 decomposition [35], which also need to be accounted for in the overall cost assessment of NH_3 cracking. Such a comparison of the overall process will be performed in a separate study.

4.7. *Underlying mechanisms of NH_3 cracking in the different reactors*

(a) *Thermodynamic equilibrium calculations*

In terms of underlying mechanisms, the linear rise of conversion with SEI, as observed for all reactors in Fig. 8 (left panel), might suggest that the NH_3 conversion proceeds mainly by thermal chemistry. In order to improve our understanding of what is driving the NH_3 conversion, we calculated the EC of NH_3 conversion as a function of temperature, assuming thermodynamic equilibrium; see Fig. 10.

The EC as a function of temperature exhibits a minimum of 58.5 kJ/mol at 451 K. Our thermodynamic equilibrium calculations show that NH_3 is fully decomposed at 700 K, in line with literature [35,44], and the energy supplied at higher temperatures goes only to gas heating. The linear increase in EC between 700 and 3000 K mostly coincides with depositing energy in the vibrational degrees of freedom of N_2 and H_2, while the sharp rise at higher temperatures is associated with the dissociation of H_2 and N_2.

We can see in Fig. 8 that in the RGA reactor, the EC stays roughly constant at ~ 340 kJ/mol as a function of SEI. This corresponds to quite a high average temperature of 3200 K, estimated based on the temperature required for this EC (see Fig. 10). A similar temperature can also be estimated for the APGD reactor at low SEI, where the EC is high, although it drops upon higher SEI. For the GAP and P2P reactor, the notably lower EC of ~ 200 kJ/mol corresponds to temperatures of about 2500 K. Interestingly, for our best EC results, the temperature should be very low (close to 1900 K for an EC of 150 kJ/mol; see Fig. 10) if the NH_3 conversion would only proceed by thermal chemistry. These results indicate that the different reactors produce substantially different plasma conditions and that non-thermal chemistry cannot be ruled out.

Fig. 11 presents the calculated temperature of NH_3 gas as a function of SEI. If we assume that all energy is deposited uniformly into the gas in the SEI range of our plasma reactors, the resulting values of the gas temperature are very low. For example, for the highest SEI values of 300 kJ/mol (reached by the APGD and RGA), Fig. 11 indicates a temperature of 3000 K, which is realistic for the warm plasmas under study. However, around SEI=100 kJ/mol (i.e., the lower range of the RGA and upper range of the GAP and P2P reactor), the temperature would only be slightly above 1000 K, while for SEI values around 10–30 kJ/mol (i.e., the lower range of APGD, P2P and GAP), the temperature would be only around 500 K. Clearly, these temperatures are too low for warm plasmas, as they should be around 3000 K [45], or even higher (i.e., 4000 K, as indicated from our OES measurements for the P2P reactor). Furthermore, such low temperatures would yield much lower EC (cf. Fig. 10) than the values observed in our reactors (cf. Fig. 8).

The reason for this discrepancy between Fig. 11 and the real temperature in our plasma reactors in this SEI range is that the energy (coming from the plasma power) is not uniformly deposited in the gas in our plasma reactors. The plasma typically has a smaller diameter than the reactor, and not all gas passes through this narrow (arc) plasma channel. Hence, this must be accounted for when trying to explain the mechanisms, which is discussed in the next section.

(b) *Fraction of gas passing through the plasma: Difference between macroscopic and "real" SEI*

In earlier work by our group, albeit for other gas conversion applications (namely CO_2 splitting and NO_x generation from air), we observed that only a limited fraction of the gas passes through the arc plasma in the GAP and P2P reactor, explaining the limited CO_2 conversion and obtained NO_x concentration, respectively [39–41]. Indeed, the gas flow rate passing through the plasma is typically smaller than the total gas flow rate, and thus, the SEI inside the plasma, i.e., the "real SEI", is larger than the macroscopic SEI, because SEI is inversely proportional with flow rate (cf. Eq. (2) in section 3). Because the conversion and EC are mainly determined by the real SEI inside the plasma and not necessarily by the macroscopic SEI, we should consider the higher SEI values of Fig. 11, which indeed correspond to a higher temperature (around 3000 K or higher), being more realistic for warm plasmas. This indicates that the temperature inside the arc plasma channel, determined by the higher real SEI, is much higher than the colder gas around it.

On the other hand, the temperature just outside the hot arc plasma will still be high enough for NH_3 conversion, so the "chemically active region" will be larger than only the arc plasma. This region and the fraction of gas passing through it should also be accounted for when

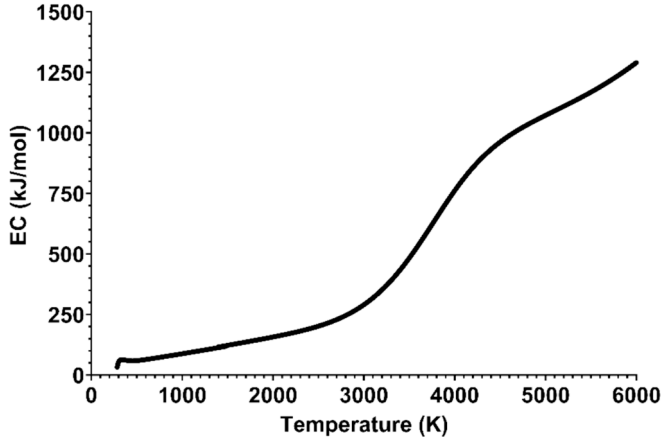

Fig. 10. Calculated EC of NH_3 conversion as a function of gas temperature, assuming thermodynamic equilibrium.

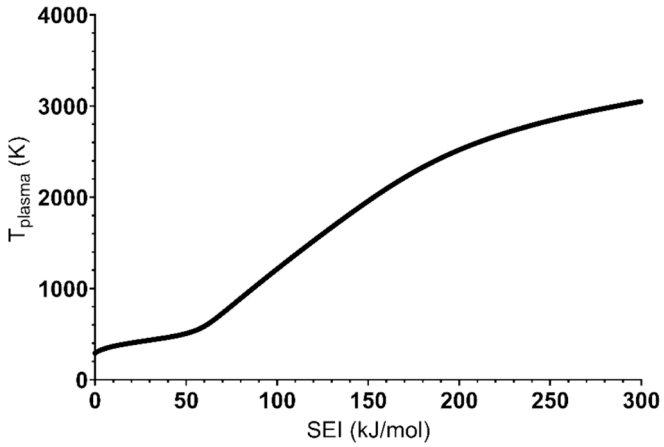

Fig. 11. Calculated temperature of NH_3 gas as a function of SEI.

considering the real SEI. As we don't know the exact diameter of the arc and of the "chemically active region" around it, we don't know the exact fraction of gas passing through the arc and through this chemically active region. Indeed, this requires detailed coupled gas flow – plasma fluid dynamics simulations, which are beyond the scope of this work. Therefore, we don't know the real SEI giving rise to NH_3 conversion in the various plasma reactors under study. For this reason, the trend of conversion as a function of macroscopic SEI, and thus also the trend of EC, is more complex, and to fully understand it, we need detailed computer simulations.

In general, increasing the macroscopic SEI, and thus the power, does not necessarily mean that the plasma arc diameter rises proportionally, because plasma contraction and power concentration are complex physical phenomena (see e.g., [46] for details). For example, in the case of the P2P reactor, the EC increases with SEI, which indicates an increase in the gas temperature (cf. Fig. 10). However, above a certain SEI, the EC stays almost constant (cf. Fig. 7) with conversion continuing to rise, suggesting that the plasma diameter increases.

In contrast to the P2P and GAP reactor, where the plasma arc is concentrated in the centre [39–41], the APGD reactor was specifically designed so that all the gas passes through the plasma by confining the plasma in a ceramic tube with a diameter similar to the calculated plasma size [37,38]. Thus, the flow rate passing through the APGD plasma is very close to the total flow rate and the real SEI inside the plasma will be very close to the macroscopic SEI. This might explain the different behaviour of EC vs SEI for the APGD reactor, as compared to the GAP and P2P reactor.

Importantly, in the GAP and P2P reactor, NH_3 decomposes both in the contracted arc plasma and in the volume of hot gas surrounding it. This means that part of the NH_3 may be converted at a lower temperature than directly inside the plasma, which may again explain the lower EC in these reactors compared to the APGD and RGA, where most of the gas passes through plasma.

(c) *Interaction between hot plasma core and surrounding colder gas, and thermal insulation*

In earlier work by our group, we have shown that the cold gas surrounding the plasma is quenching the reverse reactions, which are inhibiting CO_2 conversion [47] and NO formation [41], improving process performance. In the case of NH_3 conversion, however, the kinetic processes are much different. The reverse reaction of NH_3 decomposition, the recombination of N_2 with H_2, is mostly absent because it is an exothermic reaction that proceeds towards NH_3 formation only at lower temperatures, although it is characterised by high activation energy due to the splitting of the N_2 triple bond. This means that quenching of the product gases will not help to improve the NH_3 conversion. In other words, the underlying mechanisms driving conversion in NH_3 plasma reactors will most likely be different from the mechanisms of CO_2 splitting and NO formation from air plasmas. Notably, the mixing between the cold peripheral gas and the contracted plasma will not be a beneficial factor, as the fast temperature drop will stop the conversion.

Furthermore, because back reactions are likely not important for NH_3 cracking, the thermal efficiency of the reactor will play a major role in the chemistry and in determining the energy efficiency of NH_3 cracking. We know that the confined design of the APGD and also the narrow constriction of the RGA result in a high energy density (which may be too high for efficient NH_3 conversion; cf. Fig. 10), as well as a stronger interaction between the plasma and the walls leading to heat losses. As a result, both reactors exhibit a higher EC (around 300 kJ/mol) than the P2P and GAP reactor (around 200 kJ/mol or lower; cf. Fig. 8), which have their design optimized for thermal efficiency by utilizing a vortex gas flow in a large volume [48,49] to thermally insulate the contracted arc. A similar conclusion was obtained in [29], where operating the reactor with a swirling flow improved the performance, indicating that the flow pattern plays a crucial role in improving the reactor efficiency.

Thus, both the gas flow dynamics and thermal insulation of the hot plasma arc, as well as the fraction of gas passing through the plasma, might explain the different behaviour of EC as a function of SEI for the four different reactors, due to their distinct designs and gas flow behaviour.

(d) *Different current–voltage behaviour of the plasma reactors: Non-thermal* vs *thermal chemistry*

Obviously, there could also be other reasons for the different behaviour in the different reactors. For instance, the individual plasma reactors might have the same SEI because they have the same plasma power at the same flow rate, but they might still exhibit different electrical behaviour. Indeed, plasma power is the product of discharge voltage and current, and a high voltage/low current discharge can yield the same power as a low voltage/high current discharge, but the plasma behaviour will be different. For example, the APGD operates at a current of 25–40 mA, with a voltage of 2.2–6.3 kV, the P2P reactor operates at a current of 20–170 mA, with a voltage around 2.8–6.9 kV and the GAP reactor operates at a higher effective current of 320–560 mA, with an effective voltage around 1–2.3 kV. In other words, for the same SEI, the APGD is characterised by higher voltage/lower current than the GAP, while the P2P reactor can operate in a range of currents and voltages in between the APGD and GAP. A higher voltage typically yields a higher electric field in the plasma, which increases the electron energy, while a higher current typically results in higher electron densities. The electron energy dictates which electron impact reactions are dominant (e.g., ionisation, dissociation, vibrational or electronic excitation) and, thus, which reactive species are predominantly formed, affecting the plasma chemistry.

Based on those assumptions, we hypothesise that a higher voltage/lower current plasma might have a large contribution from non-thermal chemistry due to higher electron energies. Meanwhile, the chemistry in a lower voltage/higher current plasma will have more thermal character because of lower electron temperature, higher electron densities and higher gas temperature. In other words, the APGD might have a larger fraction of non-thermal chemistry contributing to the NH_3 conversion than the GAP and P2P reactor, and increasing the SEI might thus give rise to more efficient conversion pathways, i.e., non-thermal chemistry.

(e) *Most important electron impact and thermal NH_3 cracking reactions*

When discussing the electron impact reactions, we have to keep in mind that their role in NH_3 decomposition will depend on the plasma temperature. The importance of electron impact reactions for NH_3 cracking at low temperatures is discussed in [24].

Direct electron impact dissociation of NH_3 via high-energy electrons occurs via reaction (7):

$$e^- + NH_3 \rightarrow e^- + NH_2 + H \quad (7)$$

However, in cold plasma reactors operating in an NH_3/N_2 mixture, it has been shown that in the presence of N_2 at low temperatures, reaction (7) plays only a minor role. In those conditions, the dominant pathway for the NH_3 bond-breaking sequence, shown by reactions (8)–(11), is the dissociative quenching of $N_2(A^3)$ and $N_2(a^1)$, which are produced by electron impact excitation [24]. The importance of these reactions for the decomposition of pure NH_3 has not yet been evaluated in the literature.

$$e^- + N_2 \rightarrow e^- + N_2(A^3) \quad (8)$$

$$e^- + N_2 \rightarrow e^- + N_2(a^1) \quad (9)$$

$$N_2(A^3) + NH_3 \rightarrow N_2 + NH_2 + H \quad (10)$$

$$N_2(a^1) + NH_3 \rightarrow N_2 + NH_2 + H \quad (11)$$

On the other hand, the large rate coefficients for thermal NH_3 cracking at high temperatures (>1500 K) reported in [50] point to thermal chemistry being the dominant pathway for NH_3 decomposition. Reactions (12) and (13) are the most important ones.

$$NH_3 + M \rightleftharpoons NH_2 + H + M \quad (12)$$

$$NH_3 + H \rightleftharpoons NH_2 + H_2 \quad (13)$$

A more detailed overview of the important thermal and electron-impact reactions can be found in [24,50] and the references therein.

(f) *How to improve the NH_3 cracking efficiency? Heat recovery and reactor design improvements.*

As mentioned in section 4.4, the plasma temperature measured in the P2P reactor is around 4000 K, and similar values might be expected in the GAP reactor. This is higher than needed for thermal conversion, because thermodynamic equilibrium calculations reveal that a temperature of ~ 700 K is sufficient for nearly complete decomposition (see Fig. 10 and [35,44]). However, the time needed to reach full conversion will be excessively high, which was confirmed experimentally even a century ago [51]. Because the measured plasma temperature in the P2P reactor (and possibly also in the GAP at higher SEI) is much larger, part of the supplied energy may be wasted on overheating the gas to higher temperatures than needed for NH_3 decomposition, resulting in a significant heat loss to the environment. A possible solution could be to recycle this excess heat to preheat the gas before it enters the reactor. This reduces the plasma power used for gas heating so that it can be more efficiently used for the conversion process. Alternatively, the excess heat could be recovered and used for thermal activation of a catalyst, placed pre- or post-plasma. We will investigate these options in our future work. Finally, it is worth mentioning that the electrode material can also play the role of a catalyst, providing an additional boost to NH_3 conversion and EC, as reported in [27].

Of course, the above explanations are only hypotheses based on our general knowledge of the plasma behaviour in our different plasma reactors. Their verification requires detailed 3D (or 2D axisymmetric) computational modelling that takes into account the complex gas flow behaviour in the reactors (to evaluate whether all the gas passes through the plasma and pinpoint possible limitations in the reactor design), the complete chemistry (thermal and non-thermal electron-induced reactions), and a full coupling between gas flow dynamics and plasma behaviour. Developing such comprehensive models requires a significant amount of time, so it is beyond the scope of our paper. However, we hope our results inspire other researchers to develop such models and improve their reactor designs for enhanced cracking performance.

5. Conclusions

In this work, we investigated NH_3 cracking for green H_2 synthesis in four different warm plasma reactors, which can operate with renewable electricity: RGA, APGD, GAP, and P2P arc plasma. We compared their performance in NH_3 conversion, EC and H_2 production rate in a wide range of SEI values, determined by the plasma power and feed gas flow rate.

Overall, the GAP and P2P reactor outperform the other reactors and are interesting for further investigation. Furthermore, the P2P and GAP reactor can operate at higher NH_3 flow rates than the APGD and RGA, which results in significantly higher H_2 production rates at the same SEI. The GAP reactor is particularly stable and the NH_3 conversion can easily be increased by supplying additional energy into the plasma upon rising the SEI. However, while initially the EC of NH_3 decomposition in the GAP drops to 210–220 kJ/mol with rising SEI up to 50 kJ/mol, it does not decrease further at higher SEI, thus exceeding the lowest EC reached for thermo-catalysis (i.e., ca. 65 kJ/mol [6]) at comparable conversion. Likewise, while the EC in the P2P reactor drops upon lower SEI, achieving a minimum EC of 146 kJ/mol, it is still higher than in thermo-catalytic cracking, and at quite low NH_3 conversion of only 8 %.

All our investigated plasma reactors significantly outperform the various cold plasma reactors reported in the literature in terms of EC, and they exceed the conversion in cold plasmas without catalysts. Moreover, they are comparable to, or better than the performance of the few warm plasmas investigated already in literature. Thus, our results show that warm plasma systems are much more efficient for NH_3 decomposition than cold plasmas, even when combining the latter with catalysts.

As the measured gas temperature exceeds 4000 K in the P2P reactor, and the P2P and GAP reactor show similar conversion performance, it is highly likely that the NH_3 cracking in the P2P and GAP reactor is predominantly thermal, although non-thermal plasma chemistry may also play a role. In the case of the APGD, the behaviour is different, which may point to a larger impact of non-thermal plasma chemistry on the conversion. However, the extent of its role remains unclear. As such, we believe that the heat, characteristic of warm plasmas, plays an essential role in the NH_3 decomposition, which is an endothermic reaction. However, additional studies into the nature of NH_3 decomposition in these plasmas are needed to elucidate the underlying mechanisms. This requires 3D (or 2D axisymmetric) computational modelling, which describes the complex gas flow behaviour in the reactors, as well as detailed chemistry, including thermal and non-thermal electron-induced reactions, and a full coupling between gas flow dynamics and plasma behaviour, which is beyond the scope of our paper but is planned in our future work.

The obtained EC of plasma-based NH_3 cracking exceeds thermo-catalytic cracking by a factor of three. One of the reasons behind the higher EC in plasma reactors may be that only a limited fraction of the feed flow is treated by the plasma, as the plasma is typically confined in the centre of the reactor, and a significant fraction of the gas can pass through the reactor without passing through the plasma or plasma-heated zone [40,41,52]. Additionally, part of the energy supplied to the plasma could have been wasted on overheating the feed to higher temperatures than necessary for NH_3 decomposition, and thus, a significant amount of heat could be lost to the environment. An obvious first step to addressing these issues is designing a heat integration solution for warm plasma reactors, to recycle the excess heat into feed gas heating or as a heat source for an additional catalytic step, either pre-plasma or post-plasma.

Compared to other gas conversion applications, such as CO_2 splitting or NO_x production from air, which are also gaining increasing interest in warm plasmas [36–41,53], NH_3 decomposition presents an extra challenge for plasma reactors. The main limitation seems to arise from the higher temperatures inside the reactor, measured to be around 4000 K in the P2P reactor, and likely with similar values in the other reactors. This causes severe damage, even to the reactor components normally resistant to high temperatures, such as stainless steel (service temperature of 925 °C for SS316L) or quartz (service temperature of 1100 °C). In our future work, we will implement solutions to recover the reaction heat and reintegrate it into the process, which should alleviate this problem in our future plasma setups. Necessary modifications include a cooling system that provides a way for heat recovery and at the same time protects the reactor from thermal damage, as well as adjustment to the gas inlets and reactor geometry to increase the amount of feed that is treated by the plasma. Overall, we hope that our paper will also inspire other researchers to design improved reactors for enhanced NH_3 cracking performance.

CRediT authorship contribution statement

Igor Fedirchyk: Writing – review & editing, Writing – original draft, Visualization, Validation, Methodology, Investigation, Formal analysis,

Data curation. **Ivan Tsonev:** Writing – review & editing, Formal analysis. **Rubén Quiroz Marnef:** Writing – review & editing, Visualization, Software. **Annemie Bogaerts:** Writing – review & editing, Supervision, Project administration, Funding acquisition, Conceptualization.

Declaration of competing interest

The authors declare that they have no known competing financial interests or personal relationships that could have appeared to influence the work reported in this paper.

Data availability

Data will be made available on request.

Acknowledgements

This work was supported by the HyPACT project funded by the Belgian Energy Transition Fund and the MSCA4Ukraine project 1233629 funded by the European Union.

We are grateful to A. Nikiforov for lending us the spectrometer and our discussions regarding the estimation of plasma temperature using OES. We would also like to thank Y. Gorbanev for helping us to set up the hydrazine measurement. Finally, we thank S. Maerivoet for contributing to the interpretation of the experimental results.

Appendix A. Supplementary material

Supplementary data to this article can be found online at https://doi.org/10.1016/j.cej.2024.155946.

References

[1] European Commission. 2050 long-term strategy n.d. https://climate.ec.europa.eu/eu-action/climate-strategies-targets/2050-long-term-strategy_en (accessed November 3, 2022).
[2] S. Bosu, N. Rajamohan, Recent advancements in hydrogen storage - comparative review on methods, operating conditions and challenges, Int J Hydrog Energy 52 (2024) 352–370, https://doi.org/10.1016/j.ijhydene.2023.01.344.
[3] Hydrogen Import Coalition. Study on large-scale import of hydrogen from other continents n.d. https://www.waterstofnet.eu/en/knowledge-centre/roadmaps-and-studies/h2-importcoalition.
[4] International Renewable Energy Agency (IRENA), Ammonia Energy Association (AEA). Innovation Outlook: Renewable Ammonia. Abu Dhabi, Brooklyn: 2022.
[5] C. Chen, K. Wu, H. Ren, C. Zhou, Y. Luo, L. Lin, et al., Ru-based catalysts for ammonia decomposition: a mini-review, Energy Fuels 35 (2021) 11693–11706, https://doi.org/10.1021/acs.energyfuels.1c01261.
[6] Nielsen R. Topsoes Ammonia cracking technology – Delivering green Hydrogen 2021. https://www.ammoniaenergy.org/wp-content/uploads/2021/11/Rasmus-Topsoe-NH3-cracking-AEA-2021.pdf.
[7] G. Soucy, J.W. Jurewicz, M.I. Boulos, Parametric study of the decomposition of NH_3 for an induction plasma reactor design, Plasma Chem. Plasma Process. 15 (1995) 693–710, https://doi.org/10.1007/BF01447067.
[8] L. Wang, Y. Yi, H. Guo, X. Du, B. Zhu, Y. Zhu, Highly dispersed Co nanoparticles prepared by an improved method for plasma-driven NH_3 decomposition to produce H_2, Catalysts 9 (2019) 107, https://doi.org/10.3390/catal9020107.
[9] Z. Wang, G. He, H. Zhang, C. Liao, C. Yang, F. Zhao, et al., Plasma-promoted ammonia decomposition over supported ruthenium catalysts for CO_x-free H_2 production, ChemSusChem 16 (2023) e202202370.
[10] Y. Yi, L. Wang, Y. Guo, S. Sun, H. Guo, Plasma-assisted ammonia decomposition over Fe–Ni alloy catalysts for CO_x-Free hydrogen, AIChE J 65 (2018) 691–701, https://doi.org/10.1002/aic.16479.
[11] Y. Hayakawa, T. Miura, K. Shizuya, S. Wakazono, K. Tokunaga, S. Kambara, Hydrogen production system combined with a catalytic reactor and a plasma membrane reactor from ammonia, Int J Hydrog Energy 44 (2019) 9987–9993, https://doi.org/10.1016/j.ijhydene.2018.12.141.
[12] M. El-Shafie, S. Kambara, Y. Hayakawa, Energy and exergy analysis of hydrogen production from ammonia decomposition systems using non-thermal plasma, Int J Hydrog Energy 46 (2021) 29361–29375, https://doi.org/10.1016/j.ijhydene.2020.08.249.
[13] L. Wang, Y. Yi, Y. Zhao, R. Zhang, J. Zhang, H. Guo, NH_3 decomposition for H_2 generation: effects of cheap metals and supports on plasma-catalyst synergy, ACS Catal. 5 (2015) 4167–4174, https://doi.org/10.1021/acscatal.5b00728.
[14] L. Wang, Y. Zhao, C. Liu, W. Gong, H. Guo, Plasma driven ammonia decomposition on a Fe-catalyst: eliminating surface nitrogen poisoning, Chem. Commun. 49 (2013) 3787, https://doi.org/10.1039/c3cc41301b.
[15] Z. Wang, H. Zhang, Z. Ye, G. He, C. Liao, J. Deng, et al., H_2 production from ammonia decomposition with Mo_2N catalyst driven by dielectric barrier discharge plasma, Int J Hydrog Energy 49 (2024) 1375–1385, https://doi.org/10.1016/j.ijhydene.2023.06.173.
[16] X. Yu, K. Hu, H. Zhang, G. He, Y. Xia, M. Deng, et al., Plasma-catalytic ammonia decomposition for carbon-free hydrogen production using low pressure-synthesized Mo_2N catalyst, Plasma Chem. Plasma Process. 43 (2023) 183–197, https://doi.org/10.1007/s11090-022-10282-y.
[17] Goto Y, Hayakawa Y, Kambara S. Reaction Mechanism of Ammonia Decomposition by Atmospheric Plasma. Ext. Abstr. Ninth JSME-KSME Therm. Fluids Eng. Conf., Okinawa, Japan: 2017, p. TFEC9-1449.
[18] J.A. Andersen, J.M. Christensen, M. Østberg, A. Bogaerts, A.D. Jensen, Plasma-catalytic ammonia decomposition using a packed-bed dielectric barrier discharge reactor, Int J Hydrog Energy 47 (2022) 32081–32091, https://doi.org/10.1016/j.ijhydene.2022.07.102.
[19] Y. Hayakawa, S. Kambara, T. Miura, Hydrogen production from ammonia by the plasma membrane reactor, Int. J. Hydrog. Energy 45 (2020) 32082–32088, https://doi.org/10.1016/j.ijhydene.2020.08.178.
[20] P. Navascués, J.M. Obrero-Pérez, J. Cotrino, A.R. González-Elipe, A. Gómez-Ramírez, Unraveling discharge and surface mechanisms in plasma-assisted ammonia reactions, ACS Sustain. Chem. Eng. 8 (2020) 14855–14866, https://doi.org/10.1021/acssuschemeng.0c04461.
[21] G. Chen, J. Qu, P. Cheah, D. Cao, Y. Zhao, Y. Xiang, Size-dependent activity of iron nanoparticles in both thermal and plasma driven catalytic ammonia decomposition, Ind. Eng. Chem. Res. 61 (2022) 11436–11443, https://doi.org/10.1021/acs.iecr.2c02092.
[22] W. Zhou, W. Zhang, Y. Shan, B. Liu, K. Li, J. Ren, et al., Carbon-free hydrogen production via plasma-catalytic ammonia decomposition over transition metal-based catalysts: in situ probing by DRIFTS and SVUV-PIMS, Chem. Eng. J. 492 (2024) 152101, https://doi.org/10.1016/j.cej.2024.152101.
[23] M. Akiyama, K. Aihara, T. Sawaguchi, M. Matsukata, M. Iwamoto, Ammonia decomposition to clean hydrogen using non-thermal atmospheric-pressure plasma, Int J Hydrog Energy 43 (2018) 14493–14497, https://doi.org/10.1016/j.ijhydene.2018.06.022.
[24] S. Bang, R. Snoeckx, M.S. Cha, Kinetic study for plasma assisted cracking of NH_3: approaches and challenges, Chem. A Eur. J. 127 (2023) 1271–1282, https://doi.org/10.1021/acs.jpca.2c06919.
[25] Andersen JA, van 't Veer K, Christensen JM, Østberg M, Bogaerts A, Jensen AD. Ammonia decomposition in a dielectric barrier discharge plasma: insights from experiments and kinetic modeling. Chem Eng Sci (2023) 271 118550. doi: 10.1016/j.ces.2023.118550.
[26] M. El-Shafie, S. Kambara, Y. Hayakawa, Alumina particle size effect on H_2 production from ammonia decomposition by DBD plasma, Energy Rep. 6 (2020) 25–30, https://doi.org/10.1016/j.egyr.2020.10.032.
[27] Y. Zhao, L. Wang, J. Zhang, W. Gong, H. Guo, Decomposition of ammonia by atmospheric pressure AC discharge: catalytic effect of the electrodes, Catal. Today 211 (2013) 72–77, https://doi.org/10.1016/j.cattod.2013.03.027.
[28] M. Młotek, M. Perron, K. Krawczyk, Ammonia decomposition in a gliding discharge plasma, Energy Technol 9 (2021) 2100677, https://doi.org/10.1002/ente.202100677.
[29] Q.F. Lin, Y.M. Jiang, C.Z. Liu, L.W. Chen, W.J. Zhang, J. Ding, et al., Instantaneous hydrogen production from ammonia by non-thermal arc plasma combining with catalyst, Energy Rep. 7 (2021) 4064–4070, https://doi.org/10.1016/j.egyr.2021.06.087.
[30] Ronduda H, Młotek M, Góral W, Zybert M, Ostrowski A, Sobczak K, et al. Cobalt catalysts for COx-free hydrogen production: Effect of catalyst type on ammonia decomposition in gliding discharge plasma reactor. J CO2 Util (2024) 82 102755. doi: 10.1016/j.jcou.2024.102755.
[31] X. Zhang, M.S. Cha, Ammonia cracking for hydrogen production using a microwave argon plasma jet, J. Phys. Appl. Phys. 57 (2023) 065203, https://doi.org/10.1088/1361-6463/ad0988.
[32] A. Bogaerts, E.C. Neyts, Plasma technology: an emerging technology for energy storage, ACS Energy Lett. 3 (2018) 1013–1027, https://doi.org/10.1021/acsenergylett.8b00184.
[33] A. Fridman, S. Nester, L.A. Kennedy, A. Saveliev, O. Mutaf-Yardimci, Gliding arc gas discharge, Prog. Energy Combust. Sci. 25 (1998) 211–231, https://doi.org/10.1016/S0360-1285(98)00021-5.
[34] S.R. Sun, H.X. Wang, D.H. Mei, X. Tu, A. Bogaerts, CO_2 conversion in a gliding arc plasma: performance improvement based on chemical reaction modeling, J. CO2 Util. 17 (2017) 220–234, https://doi.org/10.1016/j.jcou.2016.12.009.
[35] I. Lucentini, X. Garcia, X. Vendrell, J. Llorca, Review of the decomposition of ammonia to generate hydrogen, Ind. Eng. Chem. Res. 60 (2021) 18560–18611, https://doi.org/10.1021/acs.iecr.1c00843.
[36] F. Jardali, S. Van Alphen, J. Creel, H. Ahmadi Eshtehardi, M. Axelsson, R. Ingels, et al., NO_x production in a rotating gliding arc plasma: potential avenue for sustainable nitrogen fixation, Green Chem. 23 (2021) 1748–1757, https://doi.org/10.1039/D0GC03521A.
[37] G. Trenchev, A. Nikiforov, W. Wang, K. St, A. Bogaerts, Atmospheric pressure glow discharge for CO_2 conversion: model-based exploration of the optimum reactor configuration, Chem. Eng. J. 362 (2019) 830–841, https://doi.org/10.1016/j.cej.2019.01.091.
[38] B. Wanten, S. Maerivoet, C. Vantomme, J. Slaets, G. Trenchev, A. Bogaerts, Dry reforming of methane in an atmospheric pressure glow discharge: confining the plasma to expand the performance, J. CO_2 Util. 56 (2022) 101869, https://doi.org/10.1016/j.jcou.2021.101869.

[39] M. Ramakers, G. Trenchev, S. Heijkers, W. Wang, A. Bogaerts, Gliding Arc Plasmatron: providing an alternative method for carbon dioxide conversion, ChemSusChem 10 (2017) 2642–2652, https://doi.org/10.1002/cssc.201700589.
[40] R. Vertongen, A. Bogaerts, How important is reactor design for CO_2 conversion in warm plasmas? J. CO_2 Util. 72 (2023;) 102510 https://doi.org/10.1016/j.jcou.2023.102510.
[41] I. Tsonev, H. Ahmadi Eshtehardi, M.-P. Delplancke, A. Bogaerts, Importance of geometric effects in scaling up energy-efficient plasma-based nitrogen fixation, Sustain Energy Amp Fuels 8 (2024) 2191–2209, https://doi.org/10.1039/D3SE01615C.
[42] C.O. Laux, T.G. Spence, C.H. Kruger, R.N. Zare, Optical diagnostics of atmospheric pressure air plasmas, Plasma Sources Sci. Technol. 12 (2003) 125–138, https://doi.org/10.1088/0963-0252/12/2/301.
[43] B. Wanten, R. Vertongen, R. De Meyer, A. Bogaerts, Plasma-based CO_2 conversion: how to correctly analyze the performance? J Energy Chem 86 (2023) 180–196, https://doi.org/10.1016/j.jechem.2023.07.005.
[44] S.-F. Yin, Q.-H. Zhang, B.-Q. Xu, W.-X. Zhu, C.-F. Ng, C.-T. Au, Investigation on the catalysis of COx-free hydrogen generation from ammonia, J. Catal. 224 (2004) 384–396, https://doi.org/10.1016/j.jcat.2004.03.008.
[45] G. Trenchev, K. St, W. Wang, M. Ramakers, A. Bogaerts, CO_2 Conversion in a gliding arc plasmatron: multidimensional modeling for improved efficiency, J. Phys. Chem. C 121 (2017) 24470–24479, https://doi.org/10.1021/acs.jpcc.7b08511.
[46] O. Biondo, A. Hughes, A. van de Steeg, S. Maerivoet, B. Loenders, G. van Rooij, A. Bogaerts, Power concentration determined by thermodynamic properties in complex gas mixtures: the case of plasma-based dry reforming of methane, Plasma Sources Sci. Technol. 32 (2023) 045001, https://doi.org/10.1088/1361-6595/acc6ec.
[47] V. Vermeiren, A. Bogaerts, Plasma-based CO_2 conversion: to quench or not to quench? J. Phys. Chem. C 124 (2020) 18401–18415, https://doi.org/10.1021/acs.jpcc.0c04257.
[48] A. Gutsol, J.A. Bakken, A new vortex method of plasma insulation and explanation of the Ranque effect, J Phys Appl Phys 31 (1998) 704, https://doi.org/10.1088/0022-3727/31/6/018.
[49] C.S. Kalra, Y.I. Cho, A. Gutsol, A. Fridman, T.S. Rufael, Gliding arc in tornado using a reverse vortex flow, Rev. Sci. Instrum. 76 (2005) 025110, https://doi.org/10.1063/1.1854215.
[50] P. Glarborg, H. Hashemi, P. Marshall, Challenges in kinetic modeling of ammonia pyrolysis, Fuel Commun 10 (2022) 100049, https://doi.org/10.1016/j.jfueco.2022.100049.
[51] C.N. Hinshelwood, R.E. Burk, CLIII.-the thermal decomposition of ammonia upon various surfaces, J. Chem. Soc. Trans. 127 (1925) 1105–1117, https://doi.org/10.1039/CT9252701105.
[52] M. Ramakers, J.A. Medrano, G. Trenchev, F. Gallucci, A. Bogaerts, Revealing the arc dynamics in a gliding arc plasmatron: a better insight to improve CO_2 conversion, Plasma Sources Sci. Technol. 26 (2017) 125002, https://doi.org/10.1088/1361-6595/aa9531.
[53] I. Tsonev, C. O'Modhrain, A. Bogaerts, Y. Gorbanev, Nitrogen fixation by an arc plasma at elevated pressure to increase the energy efficiency and production rate of NO_x, ACS Sustain. Chem. Eng. 11 (2023) 1888–1897, https://doi.org/10.1021/acssuschemeng.2c06357.

Plasma-assisted NH_3 cracking in warm plasma reactors for green H_2 production – Supporting information

Igor Fedirchyk, Ivan Tsonev, Rubén Quiroz Marnef, Annemie Bogaerts
PLASMANT, Department of Chemistry, University of Antwerp,
Universiteitsplein 1, BE-2610 Wilrijk, Antwerp, Belgium

E-mail: igor.fedirchyk@uantwerpen.be

S1. Calibration curve for determining NH_3 conversion based on values measured by H_2 TCD

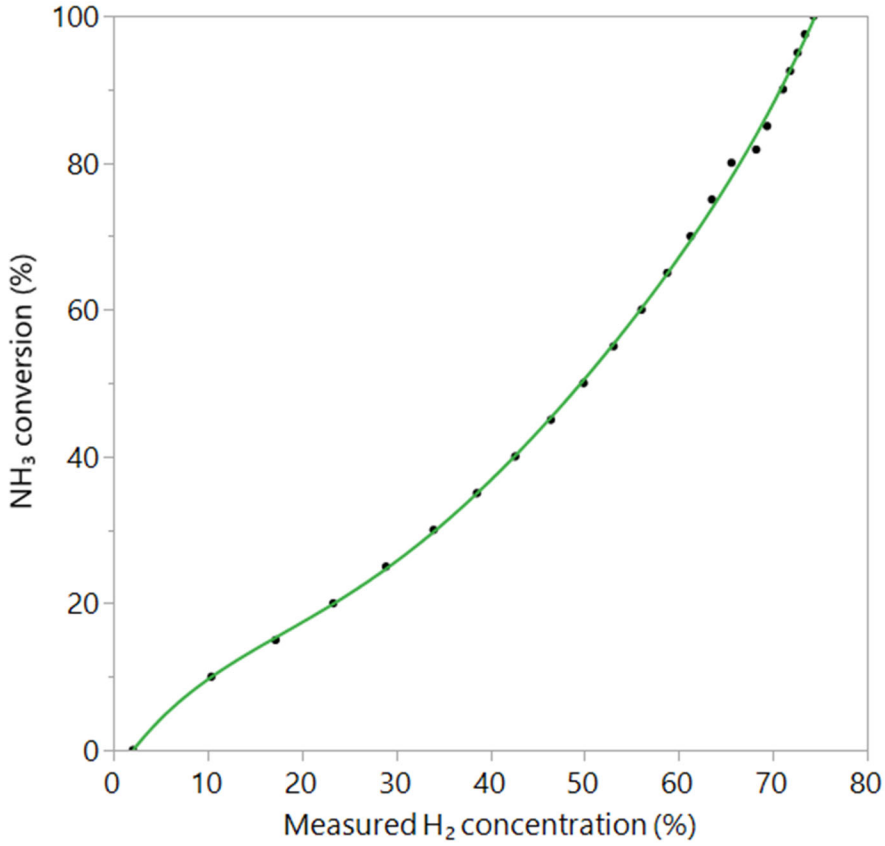

The calibration curve is approximated using a polynomial from equation S1.1:

$$X_{NH_3} = -25.25046 + 1.5156835 \cdot C_{H_2}^{TCD} + 0.0129463 \cdot \left(C_{H_2}^{TCD} - 50.1213\right)^2 + 5.3023 \cdot 10^{-5} \cdot \left(C_{H_2}^{TCD} - 50.1213\right)^3 + 7.1679 \cdot 10^{-6} \cdot \left(C_{H_2}^{TCD} - 50.1213\right)^4 + 1.5674 \cdot 10^{-7} \cdot \left(C_{H_2}^{TCD} - 50.1213\right)^5 \quad \text{(S1.1)}$$

where X_{NH_3} is the NH_3 conversion (in %) and $C_{H_2}^{TCD}$ is the H_2 concentration measured using the H_2 TCD.

S2. Measurement of hydrazine content in the products of NH_3 cracking

The hydrazine (N_2H_4) concentration ($C_{N_2H_4}^{out}$) in the exhaust gas was measured by scanning the samples in the 400–600 nm range using a UV/VIS spectrophotometer. The presence of N_2H_4 in the samples creates an absorbance maximum at 458 nm. The samples were prepared by dissolving NH_3 cracking products in 250 mL of deionised water (H_2O) using a gas washing bottle. 1 mL of the resulting liquid is pipetted into one quartz cuvette while a blank sample with 1 mL of deionised H_2O is prepared in the second cuvette. A N_2H_4 indicator is added to both samples. The concentration of N_2H_4 ($C_{N_2H_4}^{cuvette}$) in the cuvette sample is calculated based on the calibration formula S2.1:

$$C_{N_2H_4}^{cuvette}(\mu M) = 21.37 \cdot \mathrm{A} + 0.15 \quad \text{(S2.1)}$$

where A is the measured absorbance at 458 nm. Equation S2.1 was obtained from the calibration of the UV/VIS spectrophotometer for defined N_2H_4 concentrations in H_2O solutions. This was done by using seven sets of standard samples with decreasing concentrations of N_2H_4 in water (Table S2.1).

Table S2.1: The measured absorbance values based on seven standards with different N_2H_4 concentrations measured with a UV/VIS spectrophotometer.

$C_{N_2H_4}^{real}$ (µM)	Absorbance (a.u.)
59.1	2.790
39.4	1.779
29.55	1.385
19.7	0.914
9.85	0.437
4.925	0.264
1.97	0.080

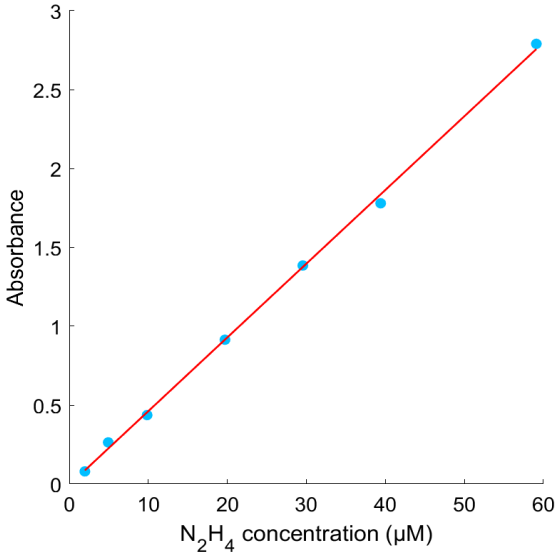

Figure S2.1. Calibration curve for UV/VIS spectrophotometer built using measured absorbance values of seven standards with different N_2H_4 concentrations.

Existing reports indicate that hydrazine production during plasma-based NH_3 decomposition is limited, so during calibration the sample with the highest concentration of N_2H_4 was prepared by dissolving 0.03 mL of a hydrazine hydrate solution (99%) in 500 mL of deionised water, after which the solution was diluted 22 times. This produces the initial sample with a hydrazine concentration of 59 µM. Six additional samples were made by diluting the first sample with deionised water 1.5, 2, 3, 6, 12 and 30 times. After an incubation time of 30 min, each sample was measured in the 400–600 nm wavelength range. A plot of the measured absorbance as a function of the real N_2H_4 concentrations (Figure S2.1) shows a linear relationship, represented by equation S2.1.

$C_{N_2H_4}^{cuvette}$ is the concentration N_2H_4 present in the cuvette sample ($V_{cuvette}$ = 1 mL). Using $C_{N_2H_4}^{cuvette}$, the total volume of liquid in the gas washing bottle (V_{GWB} = 0.25 L), the total time during which the hydrazine sample was collected (t_{sample}), and molar volume of gaseous hydrazine (V_m = 22.4 Ln/min), we can calculate the flow rate of hydrazine in the cracking products ($Q_{N_2H_4}^{out}$) via equation S2.2.

$$Q_{N_2H_4}^{out}\left(\frac{Ln}{min}\right) = \frac{C_{N_2H_4}^{cuvette}\left(\frac{mol}{L}\right) \cdot V_{GWB}\,(L) \cdot V_m\left(\frac{Ln}{mol}\right)}{t_{sample}\,(min)} \quad \text{(S2.2)}$$

By knowing the composition of cracking products, we can calculate their total flow rate (Q_{total}^{out}) and then use it and $Q_{N_2H_4}^{out}$ to find $C_{N_2H_4}^{out}$ using formula S2.3.

$$C_{N_2H_4}^{out} = \frac{Q_{N_2H_4}^{out}}{Q_{total}^{out}} \quad \text{(S2.3)}$$

A solution of NH_3 decomposition products that was used for hydrazine measurement was produced by passing the output gas at a set gas flow rate through a gas washing bottle for t_{sample} = 30 min. The analysis of the obtained solution shows that the hydrazine concentration in the NH_3 decomposition products was less than 0.0003 %. This supports our initial assumption upon which the composition of decomposition products is measured: the decomposition of NH_3 results in a mixture of H_2 and N_2 with a ratio of 3:1 with insignificant concentration of byproducts, such as hydrazine.

S3. Estimation of the rotational temperature using OES

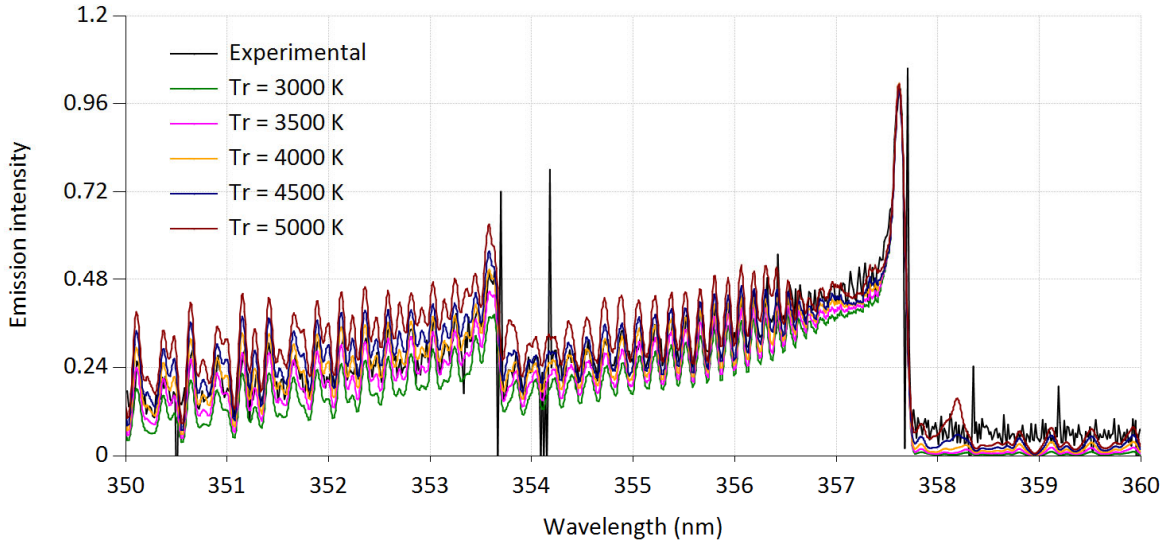

Figure S3.1. Example of SpecAir simulation of the P2P arc discharge spectrum obtained at a current of 140 mA, feed flow rate of 20 Ln/min and SEI of 68.9 kJ/mol.

Figure S3.1 illustrates the measured OES spectrum for the P2P arc discharge, as well as some simulated spectra for different rotational temperatures (see legend). The simulated spectra in the T_{rot} range from 3500 to 4500 K provided more or less the same good fit to the experimental spectrum. At T_{rot} below 3500 K and over 4500 K, the fit was significantly worse. Hence, we estimate $T_{rot} = 4000 \pm 500$ K as the gas temperature inside the core of the arc plasma channel.

S4. Thermodynamic calculations

Figure 9 in the main paper was made by finding the chemical composition at a specific temperature that minimizes the Gibbs free energy. The calculations were performed using the free software Cantera [1]. The Gibbs free energy is calculated based on the NASA9 polynomials [2] and minimized using the VCS algorithm [3].

The mixture is initialized at a specific temperature, pressure, and chemical composition. It is then equilibrated at this temperature and pressure. Based on the equilibrium composition, the energy cost (EC) is then given by equation (S4.1)

$$EC\left(\frac{kJ}{mol}\right) = \frac{\Delta H}{\mathrm{X}} = \frac{H(T) - H(T_0)}{\mathrm{X}} = \frac{\sum H_i(T) y_i - H_{NH_3}(T_0)}{\mathrm{X}} \quad \text{(S4.1)}$$

Where the sum runs over all species in the mixture and y_i is the mole fraction of the i-th species. The initial enthalpy is given by the enthalpy of ammonia at the reference temperature of 273.15 K. The conversion X is calculated by equation (4) in the main paper.

Figure 10 in the main paper is calculated by defining the specific energy input (SEI) as the change in enthalpy and plotting the corresponding temperature. This will always give a monotone increasing function since heat capacities are always non-negative [4].

The species present in the mixture are e^-, H, H^+, H_2, H_2^+, N, N^+, N_2, N_2^+, N_3, NH, NH^+, NH_2, NH_3, NH_4^+, N_2H_2, and N_2H_4. These are all the dominant neutral and positive ion species, and the electron.

The composition as a function of temperature is presented in figure S4.1.

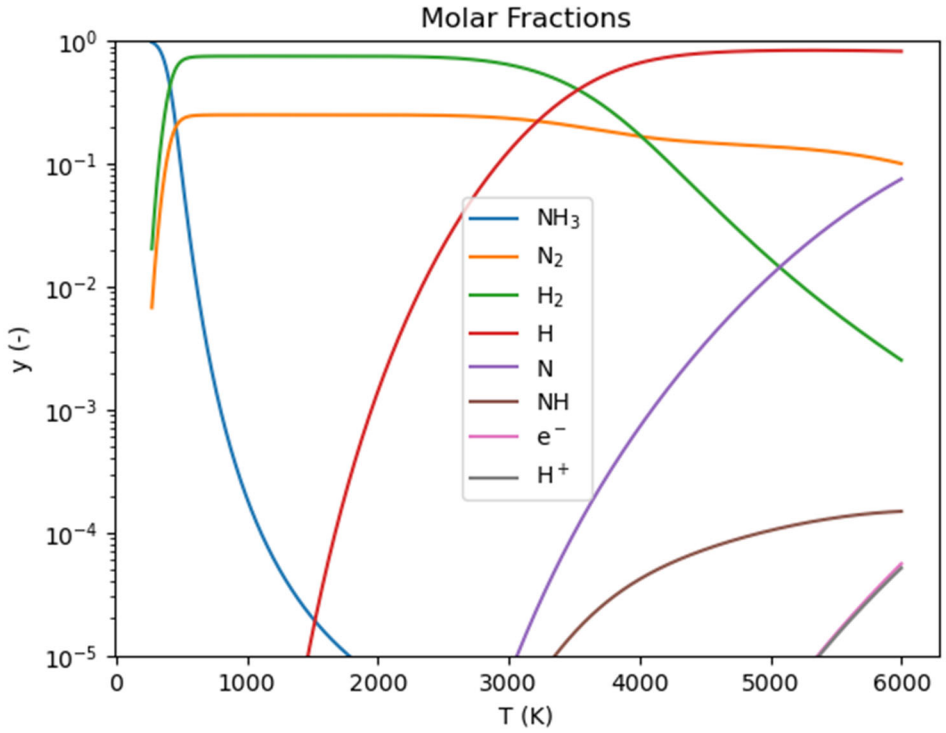

Figure S4.1 Calculated molar fractions for the species with maximal molar fraction over 10^{-5}. The legend shows what color corresponds to which species.

References

[1] Goodwin DG, Moffat HK, Schoegl I, Speth RL, Weber BW. Cantera: An Object-oriented Software Toolkit for Chemical Kinetics, Thermodynamics, and Transport Processes 2023. https://doi.org/10.5281/zenodo.8137090.

[2] McBride BJ, Zehe MJ, Gordon S. NASA Glenn coefficients for calculating thermodynamic properties of individual species. Clevelend, OH, USA: NASA Glenn Research Center; 2002.

[3] Smith WR, Missen RW. Chemical reaction equilibrium analysis: Theory and algorithms. New York, NY, USA: Wiley; 1982.

[4] Landau LD, Lifshitz EM. Statistical Physics. vol. 5. 3rd ed. Elsevier; 1980.